Swiss J Geosci (2011) 104:471–491
DOI 10.1007/s00015-011-0087-8

Eoalpine tectonics of the Eastern Alps: implications from the evolution of monometamorphic Austroalpine units (Schneeberg and Radenthein Complex)

Kurt Krenn · Walter Kurz · Harald Fritz · Georg Hoinkes

Received: 21 October 2010 / Accepted: 8 November 2011 / Published online: 25 November 2011

Abstract Monometamorphic metasediments of Paleozoic or Mesozoic age constituting Schneeberg and Radenthein Complex experienced coherent deformation and metamorphism during Late Cretaceous times. Both complexes are part of the Eoalpine high-pressure wedge that formed an intracontinental suture and occur between the polymetamorphosed Ötztal–Bundschuh nappe system on top and the Texel–Millstatt Complex below. During Eoalpine orogeny Schneeberg and Radenthein Complexes were south-dipping and they experienced a common tectonometamorphic history from ca. 115 Ma onwards until unroofing of the Tauern Window in Miocene times. This evolution is subdivided into four distinct tectonometamorphic phases. Deformation stage D1 is characterized by WNW-directed shearing at high temperature conditions (550–600°C) and related to the initial exhumation of the high-pressure wedge. D2 and D3 are largely coaxial and evolved during high- to medium-temperature conditions (ca. 450 to ≥550°C). These stages are related to advanced exhumation and associated with large-scale folding of the high-pressure wedge including the Ötztal-Bundschuh nappe system above and the Texel–Millstatt Complex below. For the area west of the Tauern Window, F2/F3 fold interference results in the formation of large-scale sheath-folds in the frontal part of the nappe stack (formerly called "Schlingentektonik" by previous authors). Earlier thrusts were reactivated during Late Cretaceous normal faulting at the base of the Ötztal–Bundschuh nappe system and its cover. Deformation stage D4 is of Oligo-Miocene age and accounted for tilting of individual basement blocks along large-scale strike-slip shear zones. This tilting phase resulted from indentation of the Southern Alps accompanied by the formation of the Tauern Window.

Keywords Eastern Alps · Eoalpine tectonics · Eoalpine metamorphism · High-pressure wedge · Indenter tectonics

Editorial handling: S. Schmid and A.G. Milnes.

K. Krenn (✉) · G. Hoinkes
Department of Mineralogy and Petrology,
Institute of Earth Sciences, Karl-Franzens-University of Graz,
Universitätsplatz 2, 8010 Graz, Austria
e-mail: kurt.krenn@uni-graz.at

W. Kurz · H. Fritz
Department of Geology and Paleontology,
Institute of Earth Sciences, Karl-Franzens-University of Graz,
Heinrichstrasse 26, 8010 Graz, Austria

1 Introduction

Austroalpine nappes, immediately located west and east of the Tauern Window show a similar evolution in terms of lithology, structure, metamorphic grade and geochronology. These nappes are part of the Middle Austroalpine nappe stack sensu Tollmann (1977), considered as part of the Upper Austroalpine basement nappes after Schmid et al. (2004) or as Lower Central Austroalpine units in the terminology of Janák et al. (2004). Large portions of these nappes experienced a polymetamorphic history lasting from pre-Variscan to Alpine times (e.g. Neubauer et al. 1999; Hoinkes et al. 1999). Some metasedimentary units within this nappe stack, however, experienced only one single phase of tectonometamorphic imprint during Alpine orogeny. These units, referred to as monometamorphic sedimentary sequences, have to be regarded as sedimentary cover resting upon a pre-Alpine basement. This study deals with the structural evolution of two of these sequences, the Schneeberg and Radenthein Complex, now located west and east of the Tauern Window, respectively (Fig. 1). Our

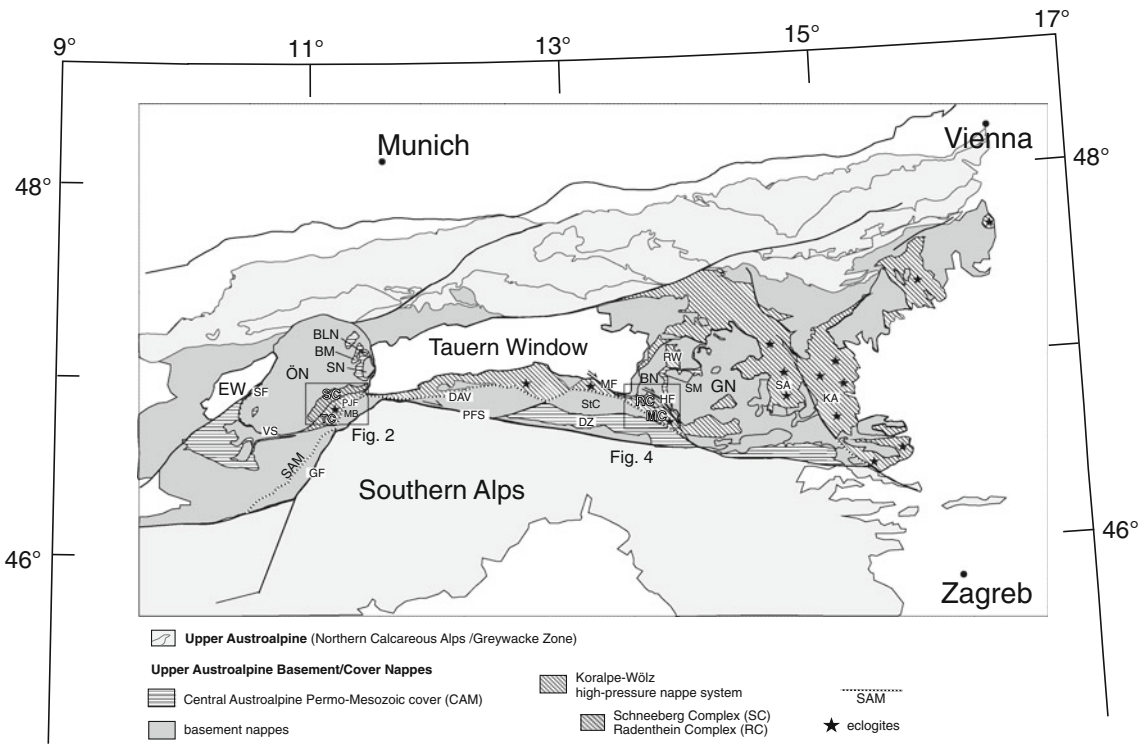

Fig. 1 Simplified geological overview of the Eastern Alps including the main tectonic nappe subdivision after Schmid et al. (2004). *EW* Engadin Window, *ÖN* Ötztal nappe, *SN* Steinach nappe, *BLN* Blaser nappe, *BM* Brenner Mesozoic, *SC* Schneeberg Complex, *TC* Texel Complex, *SF* Schlinig Fault, *VS* Vinschgau Shear Zone, *PJF* Passeier–Jaufen Fault, *MB* Meran-Mauls Basement, *PFS* Periadriatic Fault System, *DAV* Defferegggen–Antholz–Vals Fault, *BN* Bundschuh nappe, *HF* Hochstuhl Fault, *MF* Mölltal Fault, *SM* Stangalm Mesozoic, *RC* Radenthein Complex, *MC* Millstatt Complex, *DZ* Drauzug, *RW* Rammingstein Window, *GN* Gurktal nappe, *SA* Saualpe, *KA* Koralpe, *StC* Strieden Complex

analysis of the structural evolution of these monometamorphic sequences lends support to their common paleogeographic origin and similar tectonic evolution since Cretaceous times, as proposed by Frisch et al. (2000), and will improve our understanding of processes that led to their present-day spatial separation during the Late Alpine formation of the Tauern Window.

The Schneeberg Complex (SC) is overlain by the Ötztal nappe characterized by greenschist/amphibolite facies Cretaceous ("Eoalpine") metamorphism and underlain by the Texel Complex (TC) characterized by amphibolite- to eclogite-facies Eoalpine metamorphism. The Radenthein Complex (RC) is overlain by the Eoalpine greenschist/amphibolite facies metamorphosed Bundschuh nappe and underlain by the Eoalpine amphibolite- to eclogite-facies Millstatt Complex (MC). According to Schmid et al. (2004) both complexes, the SC and RC together with the units below (TC and MC) are part of the Koralpe–Wölz high-pressure nappe system and hence define an intracontinental suture within the Austroalpine unit (Fig. 1).

The structural evolution of Austroalpine nappes is largely controlled by the interplay between phases of convergence and extension (Schimana 1986; Froitzheim et al. 1994, 1997). The Alpine nappe stack formed during Cretaceous times by WNW-directed (Ratschbacher 1986) to N-directed thrusting (Kurz and Fritz 2003). Subsequent extension released ESE-directed normal faulting accompanied with the first phase of exhumation from Late Cretaceous to Paleogene times between 90 and 60 Ma (Froitzheim et al. 1997; Fügenschuh et al. 2000; Liu et al. 2001) (Fig. 1).

Correlation problems arise from different overall orientations (strike and dip) and structural positions of the various units within the western and eastern sectors of the Koralpe–Wölz high-pressure nappe system. Lithotectonic boundaries are generally N-dipping in the west but S-dipping east of the Tauern Window, i.e. within the units of the Sau and Koralpe. This differing geometry was attributed to the effects of south-directed thrusting according to a retro-wedge geometry in the west (Sölva et al. 2005), and to northward thrusting related to a pro-wedge geometry in the east (Wiesinger et al. 2006). This same difference can also, however, be explained by late-stage indentation of the Southern Alps and associated development of a triple junction between the European plate, the Adriatic microplate and a Pannonian fragment since around 20 Ma (e.g. Lippitsch et al. 2003; Kissling et al. 2006; Brückl et al. 2010).

In spite of the differences in orientation and position of SC and RC, respectively, the arguments for their common

history are (1) identically sized garnets within Ötztal and Bundschuh nappe with a clear "jump" in X(Ca) between cores and rims; (2) a bell-shaped chemical zonation pattern in garnets of the SC and the RC; (3) the presence of paragonite amphibolites within SC and RC; (4) the replacement of diopside by tremolite within marbles of the southern TC and MC, and (5) equivalent minimum *PT* conditions for the eclogites in the TC and MC (12–14 kbar, 600–630°C) (Hoinkes 1981; Koroknai et al. 1999; Teiml et al. 1995; Teiml and Hoinkes 1996; Habler et al. 2006).

Here we present a tectonic study in support of a common tectonometamorphic evolution of SC and RC. By also considering the surrounding Upper Austroalpine basement nappes we will propose a new tectonic model for the evolution of the central Eastern Alps. The rocks from the two study areas are particularly suitable because they are free of relics of pre-Alpine deformation and metamorphism.

2 Geological setting and regional geological overview

Within the Upper Austroalpine basement nappes the grade of Eoalpine metamorphic imprint reached eclogite facies in the southern part of the Koralpe–Wölz high pressure nappe system (Hoinkes 1981, 1986; Thöni 1981; Purtscheller and Rammlmair 1982; Hoinkes et al. 1999, 2010; Faryad and Hoinkes 2003; Janák et al. 2004; see Fig. 1). Both the SC and RC, together with the adjacent eclogite bearing TC and MC are parts of this high-pressure nappe system that is tectonically juxtaposed along its southern margin by fault zones that were active in Paleogene times (e.g. Passeier–Jaufen Fault (PJF), Defferegggen–Antholz–Vals Fault). These faults are related to the early evolution of the Periadriatic Fault System (PFS) (Mancktelow et al. 2001; Müller et al. 2001) (Fig. 1), and they delineate the so-called Southern Limit of Alpine Metamorphism (SAM-Line) (Hoinkes et al. 1999). The SAM-Line separates units with Eoalpine metamorphic imprint in the north from Eoalpine weakly to non-metamorphosed units in the south (Fig. 1).

In the north, the SC and RC are overlain by the polymetamorphic Ötztal and Bundschuh nappe, respectively. East of the Tauern Window, the RC appears again further north within tectonic windows, e.g. the "Rammingstein Window" (Schuster and Frank 1999, RW in Fig. 1). Despite a general late-stage and low-grade Alpine overprint both SC and RC are still seen to have been affected by Eoalpine metamorphism as is indicated by the growth of staurolite (Hoinkes 1981; Hoinkes et al. 1999; Schuster and Frank 1999). Staurolite stability is also evident for the paragneisses of the TC, which occur further south adjacent to the SC (Fig. 2).

A parautochthonous low- to medium-grade metamorphosed Permo-Mesozoic cover overlies Ötztal and Bundschuh nappe: the so-called Brenner Mesozoic (BM) west of and the Stangalm Mesozoic (SM) east of the Tauern Window (Tollmann 1977) (Fig. 1). The uppermost elements of the nappe pile comprise the Steinach nappe (SN) west of and the Stolzalpen and Murau nappe, parts of Gurktal nappe (GN), east of the Tauern Window. These are built up by low-grade Paleozoic sequences. In the west, the Blaser nappe (BLN), comprising low-grade Mesozoic sedimentary sequences, is considered as an independent nappe between the Steinach nappe on top and the Brenner Mesozoic at the base (Oberhauser 1980). Together with the Strieden Complex (StC) and its low-grade cover (Drauzug: DZ) in the south the Gurktal nappe constitutes the Drauzug–Gurktal nappe system (DGN) (Schuster et al. 2004). The equivalent of the StC in the west is found in form of the Meran-Mauls basement and its Triassic cover sequences (MB in Fig. 1), and also the Blaser and Steinach nappe west of the Tauern window are part of the DGN.

A pre-Variscan event in the Ötztal nappe is evident from gabbros of MORB-type affinity yielding Sm-Nd formation ages between 530 and 520 Ma (Miller and Thöni 1995; Thöni et al. 2008) and 490 ± 9 Ma old migmatites (Klötzli-Chowanetz et al. 1997). Within the central parts, Rb–Sr whole rock ages derived from acidic orthogneisses range between 485 and 420 Ma (Thöni 1999). Variscan eclogites with PT conditions up to 27 kbar and ca. 730°C (Miller and Thöni 1995) and a well preserved Variscan amphibolite facies metamorphic overprint have been documented from the north-western and central parts of the Ötztal nappe (Bernhard et al. 1996; Kaindl et al. 1999; Tropper and Hoinkes 1996). In central parts of the SC, however, Konzett and Hoinkes (1996) obtained Eoalpine-age equilibrium PT conditions of 550–600°C and 8–10 kbar for paragonite-bearing amphibolites. The timing of garnet growth in micaschists of the SC ranges between 93.1 ± 4.7 and 90.0 ± 4.1 Ma (Sm-Nd age data). Rb-Sr ages of 76.0 ± 0.7 Ma from syn-kinematic white mica indicate top-to-the WNW shearing during that time range (Sölva et al. 2005). In the southern Texel Complex, Eoalpine eclogites experienced pressures between 12 and 14 kbar and temperatures of 540–620°C (Hoinkes et al. 1991; Habler et al. 2006). Eclogite crystallization occurred at about 85 ± 5 Ma (Habler et al. 2006).

PT estimates and geochronology within the Austroalpine basement nappes east of the Tauern Window were summarized by Neubauer et al. (1987) and Schuster and Frank (1999). Orthogneisses of the Bundschuh nappe give Rb-Sr whole rock and Rb-Sr muscovite cooling ages of 372 ± 29 (Hawkesworth 1976) and 352 ± 4 Ma (Frimmel 1987), respectively. Temperature conditions during Variscan metamorphism were >600°C (Frimmel 1988). Eoalpine metamorphic conditions in parts of the Bundschuh nappe reached 630°C and 10 kbar (Koroknai et al. 1999). Within the RC the Eoalpine PT conditions are around 620°C and ca. 11 kbar (Koroknai et al. 1999; Kaindl and Abart 2002).

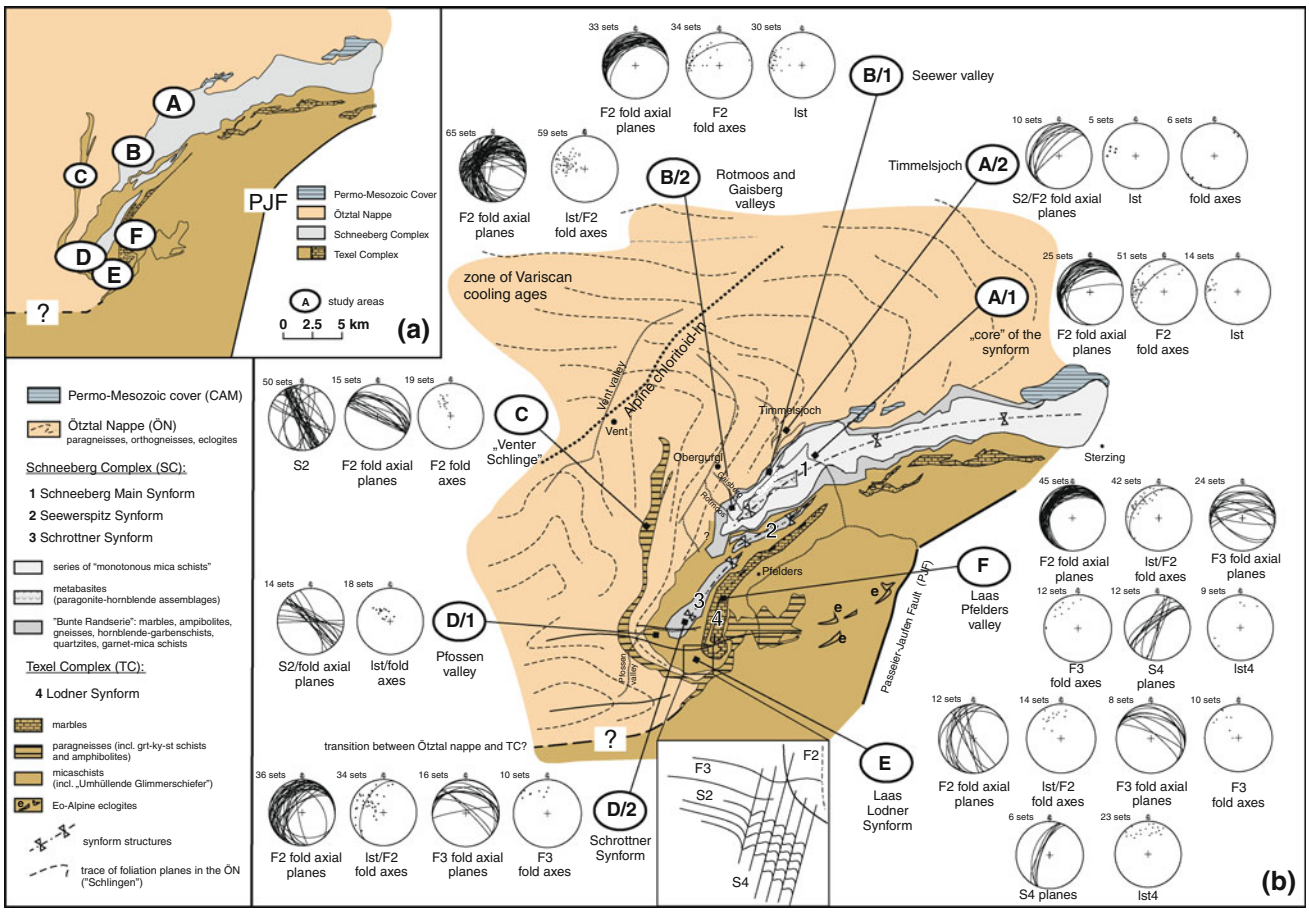

Fig. 2 **a**, **b** Major lithologies of the Schneeberg Complex and the trace of foliation planes of the surrounding areas (compilation after Schmidegg 1964; Purtscheller 1978; Helbig and Schmidt 1978; Mauracher 1980). Structures within selected study areas *A*–*F* are plotted as lower hemisphere stereographic projections. See text for details. *PJF* Passeier–Jaufen Fault, *ÖN* Ötztal nappe, *SC* Schneeberg Complex, *TC* Texel Complex

Metamorphic conditions within the Eoalpine eclogites of the southern Millstatt Complex are ≥12 kbar (X_{Jd} 40) and about 600°C according to garnet-clinopyroxene thermometry (Teiml et al. 1995). Alpine and Paleogene tectonics within the Austroalpine units east of the Tauern Window include W- to NW-directed shearing during late Early Cretaceous time overprinted by N–S shortening with steeply dipping fold axial planes (Schimana 1986; Belocky 1987). Subsequent deformation is characterized by SE-directed extension that affected the whole nappe pile during the Late Cretaceous (Genser and Neubauer 1989). Miocene overprint includes localized shearing and faulting (Ratschbacher 1986).

3 Macro- and meso-scale structures

3.1 Structures west of the Tauern Window

From top to base, Ötztal nappe, Schneeberg Complex (SC) and Texel Complex comprise a predominantly northwest to northward dipping nappe stack. In the SC, macro-scale folding defines four synforms named after Mauracher (1980) and Frank et al. (1987): Schneeberg Main Synform and Seewerspitz, Schrottner and Lodner Synforms; see Fig. 2). Looking at the trace of the main foliation mapped by Purtscheller (1978), the W–E trending foliation typical for most of the Ötztal nappe is bent when approaching the SC, i.e. within an area south of the Alpine-age chloritoid-in isograd after Thöni (1981) (see Fig. 2). Hence it is likely that the W–E-trending Variscan foliation of the Ötztal nappe has been modified (bent) in the vicinity of the Eoalpine metamorphosed SC. This is taken as an important argument that the large-scale "Schlingen"-type (Schmidegg 1964) folding in the SC must be of Eoalpine age. It is further suggested that together with this bending, previously formed W–E trending structures were rotated into an approximate N–S strike. Macro-scale fold interference patterns in the Pfossen valley result from structural overprint dominant in the southern Lodner Synform as part of the Texel Complex and in the southern Schrottner Synform as part of the SC (Schmid and

Haas 1989; Zanchi et al. 2009). Figure 2a shows the main tectonic boundaries between the Ötztal nappe, the SC and the TC. According to the geological maps after Schmidegg (1932, 1964), Purtscheller (1978) and Mauracher (1980) Eoalpine garnet–staurolite–kyanite schists of the Texel Complex are commonly folded together with the rocks of the Ötztal Complex. The so-called enveloping micaschists ("Umhüllende Glimmerschiefer" after Schmidegg 1964) found along the Pfossen valley surround the Schrottner and Lodner Synforms and are in fact part of the TC rather than belonging to the Ötztal nappe. Also the paragneisses of the Venter "Schlinge" are part of the TC (Fig. 2). Hence the boundary between the ÖC and the TC is folded around these later-stage synforms (Zanchetta et al. 2007). As a result when going from the NW to the SE one traverses rocks of the Ötztal nappe, the TC of Vent, the Ötztal nappe again, the SC and finally the TC. This geometrical complexity was formerly referred to as "Schlingentektonik" (Schmidegg 1964).

On the basis of field observations four deformation stages D1–D4 are distinguished. The three continuous stages of folding F1, F2 and F3 were followed by a stage of local mineral growth.

1. D1 is characterized by WNW-directed shearing and folding (F1), mainly preserved as S1 inclusion patterns in garnet poikiloblasts and porphyroblasts that were incorporated into subsequent fold structures.
2. D2 is characterized by folding (F2) and WNW-directed shearing parallel to the main plunging direction of the stretching lineation. D2-folding resulted in large-scale S-, Z- and M-shape intrafolial fold structures, forming the major internal structure of the SC. F2 intrafolial folds are locally non-cylindric and have NE–SW- to N–S-striking axial planes. Fold axes define a curved fold hinge line, indicative for sheath fold geometries. Related fold axial planes are parallel to the main foliation S2. Non-cylindrical folds are absent in the Ötztal nappe as well as south of the Lodner Synform (Fig. 2b).
3. D3 is non-penetrative and associated with open folding F3 with axial planes perpendicular to the earlier F2 fold structures. This resulted in type 3 fold interferences as defined by Ramsay and Huber (1987). D3 structures occur mainly in the southern part of the SC and in the southern Lodner Synform as part of the marble unit of the TC (Fig. 2b). Hence F2/F3 fold interference was responsible for the formation of the large-scale synforms.
4. D4 structures occur predominantly in the southern study areas. D4 is characterized by NW–SE shortening linked with orogen-parallel extension and SW-directed shearing. It resulted in S–C fabrics formed under semiductile/brittle conditions and into a steep-dipping S4 crenulation cleavage with NE–SW strike. The strike direction is parallel to the strike of the PJF (Fig. 2b).

Within the general tectonic scheme some domains within the SC have deviating characteristics that result from the variable intensity of particular tectonic phases. These specific local features are considered to be important for resolving the overall structure of the SC and surrounding units. Six study areas (Fig. 2a) were examined in detail and are briefly discussed below:

Study area A/1: In the "core" of the Schneeberg Main Synform (synform 1 in Fig. 2b) non-cylindrical folds F2 with S-, Z- and M-shape geometries include an earlier fabric S1 (Fig. 3a). Related F2 fold axes scatter in their orientations between SW and NE and form a curved F2-fold hinge line ("F2 fold axes" in Fig. 2b). The associated axial plane cleavage parallels S2 and trends mainly from NE–SW to N–S ("F2 fold axial planes" in Fig. 2b). The stretching lineation plunges consistently to the west.

Study area A/2: Gneisses and metabasites of the Ötztal nappe in the Timmelsjoch area show an early foliation of a probable pre-Alpine age that is incorporated into large-scale SE-vergent folds with subhorizontal NE–SW trending fold axes (D2) (Fig. 2). Related fold axial planes are parallel to the foliation S2. Folds characterize class 2 similar folds after Ramsay and Huber (1987) (Fig. 3b). Locally, chlorite-biotite schists contain S–C-fabrics and indicate displacement towards NW (inlet in Fig. 3b). A shallow NW-plunging stretching lineation revealed by hornblende and chlorite indicates lower amphibolite to greenschist facies metamorphic grade during this event.

Study area B/1: The Seewer valley exposes the transition between the Ötztal nappe and the SC ("Bunte Randserie", see Fig. 2b). Structures are almost comparable to study area A/1. Additionally, phyllonites containing mineralized quartz veins indicate late stage SW–NE-directed extension (Fig. 3c). Tight crenulation folds and garnet porphyroclasts (σ-type clasts) suggest shearing to the SW, perpendicular to the main stretching lineation (deformation stage D4, see Fig. 3d).

Study area B/2 is located nearby the fold hinge of the Schneeberg Main Synform (Rotmoos and Gaisberg valleys, Fig. 2). Meter-scale M-shape intrafolial fold structures (F2) occur in sections perpendicular to the direction of stretching (WNW) and predominate the structural content within marbles and calcareous garnet-hornblende-bearing gneisses (Fig. 3e). F2 fold axial planes differ in strike between N–S and E–W, being particularly characteristic for the hinge area of the Schneeberg Main Synform. WNW-plunging fold axes show almost the same plunge directions as the stretching lineations. Layers containing garnet and hornblende porphyroblasts are arranged as intrafolial folds of

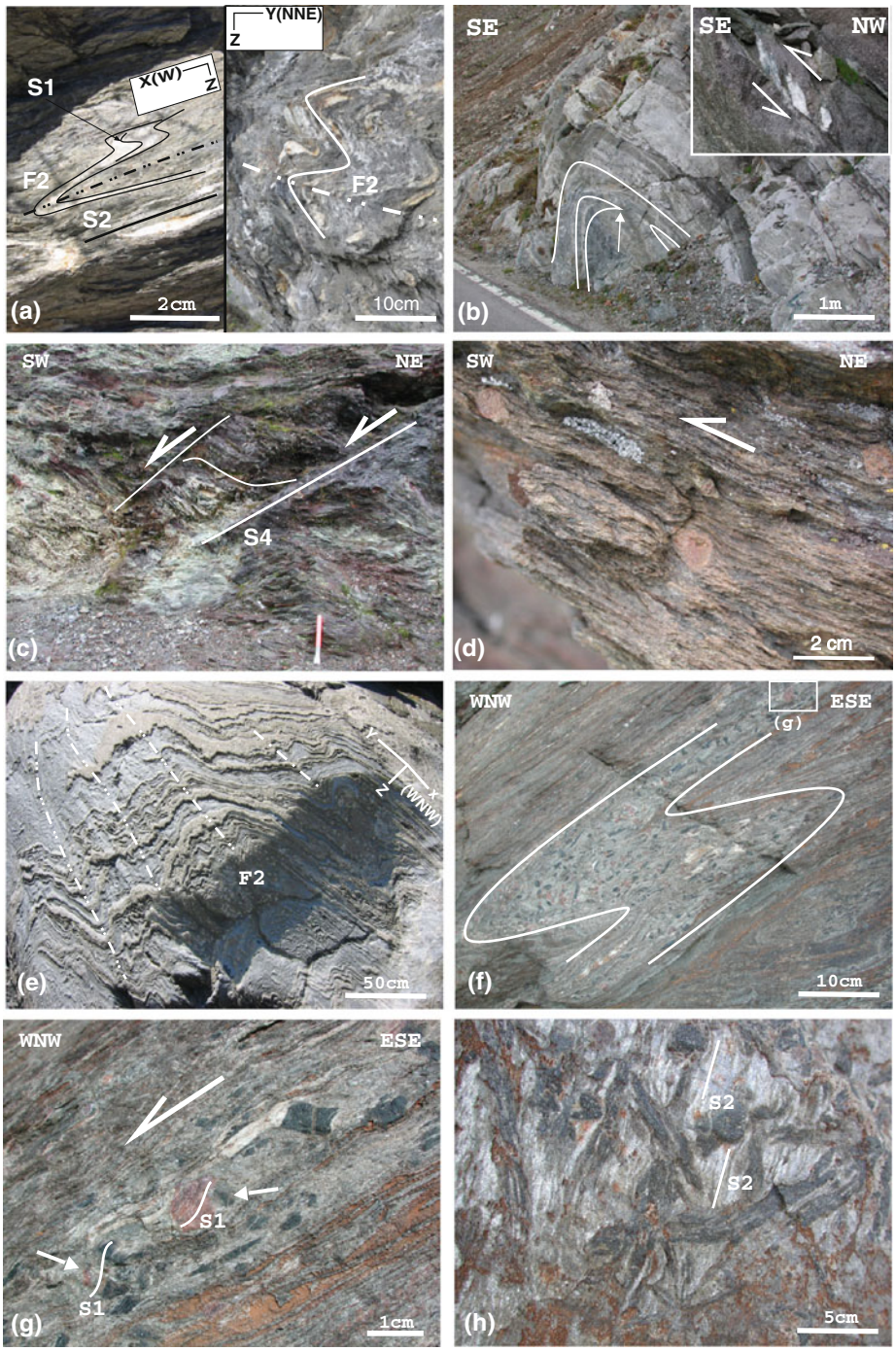

Fig. 3 **a** F2 intrafolial isoclinal fold (S-shape) in x–z and open folds (M-shape) in y–z within the series of "monotonous mica schists" (study area A/1). **b** Large-scale SE-vergent open fold in ortho- and metabasic gneisses of the Ötztal nappe. Note, early pinch-and-swell structures (*arrow*) occur incorporated in large-scale folds (study area A/2). Detail shows S–C fabric indicating NW-side-up displacement. **c** D4-extensional crenulation cleavage in mineralized phyllites (study area B/1). **d** SW-directed shear overprint in metapelites of the Seewertal valley (D4) (study area B/1). **e** M-shape intrafolial fold structure F2 within marbles in the Gaisberg valley (fold hinge area of the Schneeberg Main Synform). Note, folds occur in x–z and y–z sections (study area B/2). **f** S-shape intrafolial fold structure F2 includes earlier structures (D1) in garnet and hornblende porphyroblasts and -clasts. **g** Detail of (**f**). D1-related garnet porphroblast and hornblende aggregates with asymmetric pressure shadows. Sense of shearing is to the WNW (study area B/2). **h** D2-postdeformative growth of hornblende (study area B/2). **i** F2-intrafolial non-cylindrical fold structures in sections parallel and perpendicular to the direction of stretching (calcareous metabasites, study area D/2). **j** F3 open- to closely-spaced folds in retrogressed calcareous micaschists (study area D/2). **k** Detail in (**m**) shows F3 open folding. **l** S–C fabric south of the Lodner Synform (study area E). **m** Fold hinge area of the marble synform shows F2/F3 fold interference and S4 foliation. **n** Closely spaced crenulation folds south of the Lodner Synform (study area E). **o** S4 within paragneisses at study area F. Direction of shear overprint is to the SSW

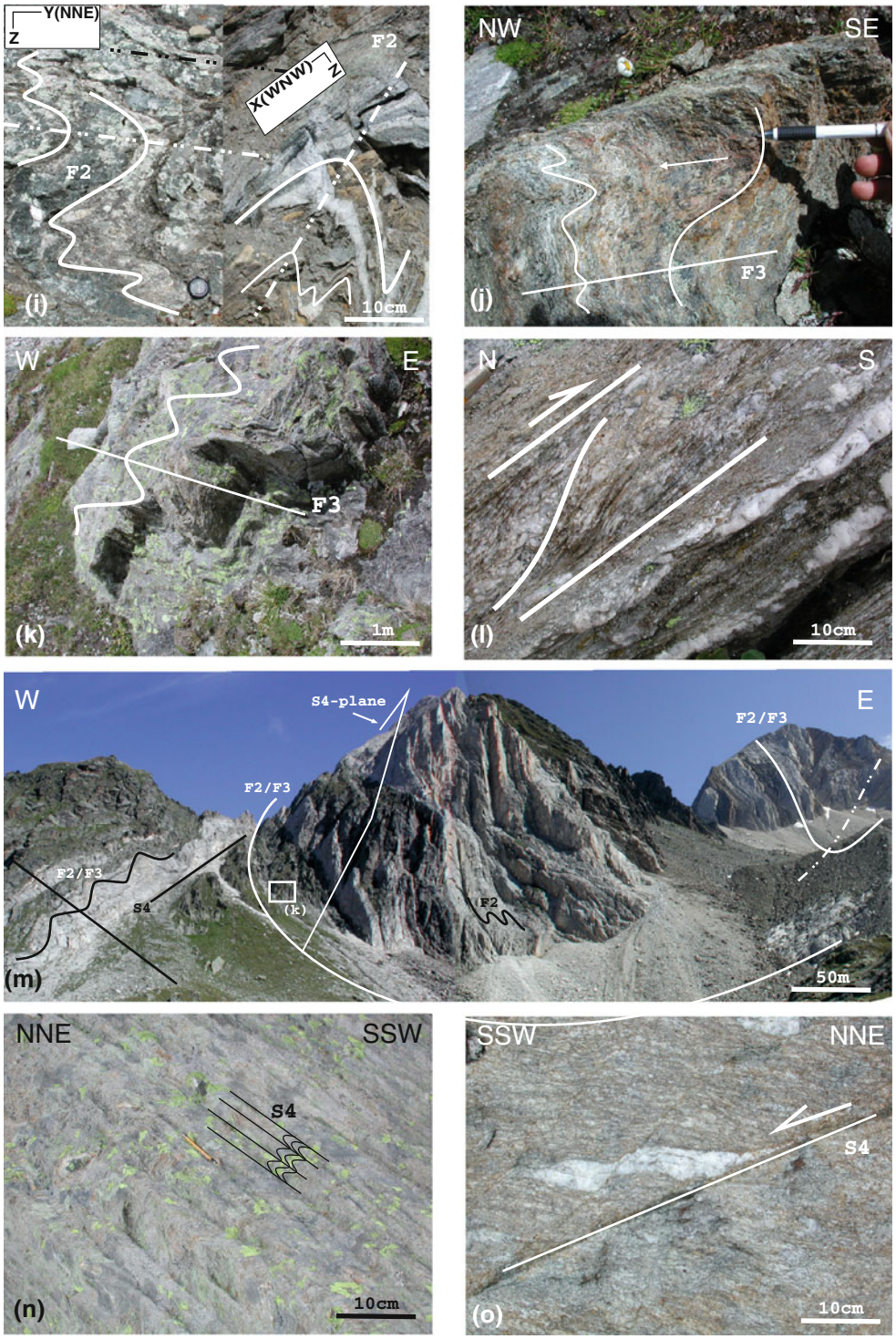

Fig. 3 continued

the large-scale synform (S-shape in Fig. 3f). Both minerals show an internal foliation S1 (Fig. 3g). D2 structures were locally overgrown by a second generation of garnet and hornblende aggregates (Fig. 3h).

At study area C, located south of Vent, the so-called "Venter-Schlinge" (Schmidegg 1964) is exposed. The foliation shows intense bending and strikes between NE–SW and NW–SE. It is folded around steep NW-plunging

fold axes (Fig. 2b). On the basis of mineral assemblage (garnet–staurolite–kyanite schists) and petrographical observations (garnets show inclusion-rich cores and inclusion poor rims as well as synkinematic recrystallization into asymmetric aggregates), these lithologies are related to the Texel Complex (Fig. 2a).

Bending in strike direction of the foliation S2 from NE–SW (study area A) to NW–SE (study area C) is observed (Fig. 2). This change in orientation goes along with steepening of the fold axes of F2 intrafolial folds with WNW–ESE-striking axial planes.

Study area D/1 located in the Pfossen valley contains micaschists of the enveloping micaschists ("Umhüllende Glimmerschiefer") and shows structures comparable to study area C. F2 fold axial planes are parallel to the foliation and almost vertical. Fold axes plunge steeply to the NW. The strike direction of the foliation indicates a further shift from NW–SE towards W–E (Fig. 2).

At study area D/2 carbonate-hornblende schists and metabasites occur in the southern part of the Schrottner Synform (synform 3 in Fig. 2). Structures are comparable to study areas A/1, B/1 and B/2. F2 fold axes scatter in plunge direction between SW and NE, suggesting a fold hinge line characteristic for F2 non-cylindrical folds (Fig. 3i). Additionally, structures were refolded by F3 open- to tightly-spaced crenulation folds (Fig. 3j). F3 fold planes strike almost E–W and are south-vergent (Fig. 2). Plunge direction of F3 fold axes is between N and NW. Refolding leads to fold interference patterns of type 3 after Ramsay and Huber (1987).

Study area E represents the southwestern part of the Lodner Synform (synform 4 in Fig. 2) and contains metapelites, metabasites and the marble unit of the TC. Due to intense folding no clear tectonic transition between the SC and the marble unit can be observed. Like in study area D/2, F2 folds are refolded by SSW-vergent open- to closely-spaced folds (F3) with NW-plunging fold axes (Fig. 3k). Locally observed F3 axial planes contain S–C fabrics, which indicate top-to-S displacement at greenschist facies conditions (deformation stage D4; Fig. 3l). Macroscale D2–D4 structures at study area E are shown in Fig. 3m. In addition, almost vertical NNE–SSW-striking foliation planes S4 occur (Fig. 3n; see sketch in Fig. 2). D4 crenulation cleavage contains a shallow around N-plunging stretching lineation (lst4) parallel to the fold axes of the locally developed crenulation folds. S4 planes trace parallel to the adjacent Passeier–Jaufen Fault (PJF in Fig. 2).

Study area F northwest of the Pfelders Valley represents the northeastern prolongation of study area E and shows large-scale F2 folding. Like study area E, all previous structures were overprinted by D3 and D4 at greenschist facies conditions. SSW-directed shear goes along with D4 (Fig. 3o).

3.2 Structures east of the Tauern Window

The Bundschuh nappe and the structurally lower Radenthein and Millstatt Complexes comprise a largely NE- to N-ward dipping succession with the Bundschuh nappe on top and the Millstatt Complex at the base (Fig. 4a). Structures in the RC are comparable to those of the SC. Deformation stage D1 is preserved as relics in micaschists in the form of an internal foliation S1 within garnet porphyroblasts (Fig. 5a). In sections parallel to the ESE-plunging stretching lineation, sigmoidal trails define shearing to the WNW (see Sect. 4.2). The external foliation (S2) is overprinted by post-kinematic mineral growth of hornblende and retrogressed garnet rims. Beside a general shift in the strike of the main foliation from W–E in the northern part to NW–SE in the southeast of the RC, the change from almost N–S at study area G towards NW–SE in study area I would possibly indicate the M-shape of a large-scale synform (Fig. 4b). Large-scale folds with NW-plunging fold axes (F2) are superposed by a second folding event F3. The latter is characterized by small-scale open folds oriented perpendicular to F2 (type 1/2 after Ramsay and Huber 1987) (study area G, Figs. 4b, 5b). For the whole RC a shift in strike direction of the foliation S2 from almost W–E in the central parts (study areas G and H) to NW–SE in the eastern and southeastern parts (study areas I and J) is observed. This goes along with steepening of the stretching lineation (lst) and fold axes (F2) from the west towards the southeast. Additional structural features in selected study areas are described below:

In study area G, almost W–E extension is indicated by small, kyanite-bearing quartz veins which developed within tensional segments, cutting foliation S2 (Fig. 5c).

In study area H, the foliation S2 is parallel to the fold axial planes F2 and strikes almost W–E. F2 fold axes suggest a W–E trending fold hinge line (Fig. 4b). Non-cylindrical F2 folds occur in gneisses and metabasites (Fig. 5d). In micaschists, open-spaced F3 folds show almost W plunging fold axes (Fig. 5e).

In study area I, nearby the transition between the RC and the Bundschuh nappe, the steep dipping foliation S2 (F2 fold axial planes) reflects a slight rotation in strike direction from WNW–ESE to NW–SE (Fig. 4b).

In study area J, non-cylindrical, open to tight intrafolial folds F2 occur (M-shape: Fig. 5f). F2 fold axes suggest a fold hinge line and related axial planes strike NW–SE (Fig. 4b). Rims of garnet porphyroblasts indicate post-deformative growth related to F2 folding (arrows in Fig. 5g). Meter-scale extensional quartz veins with NE–SW strike direction cut the foliation S2 at high angles (Fig. 5h). High-angle normal faults indicate extension to the east (D4). Fault planes strike from NNW–SSE to N–S (Fig. 4b).

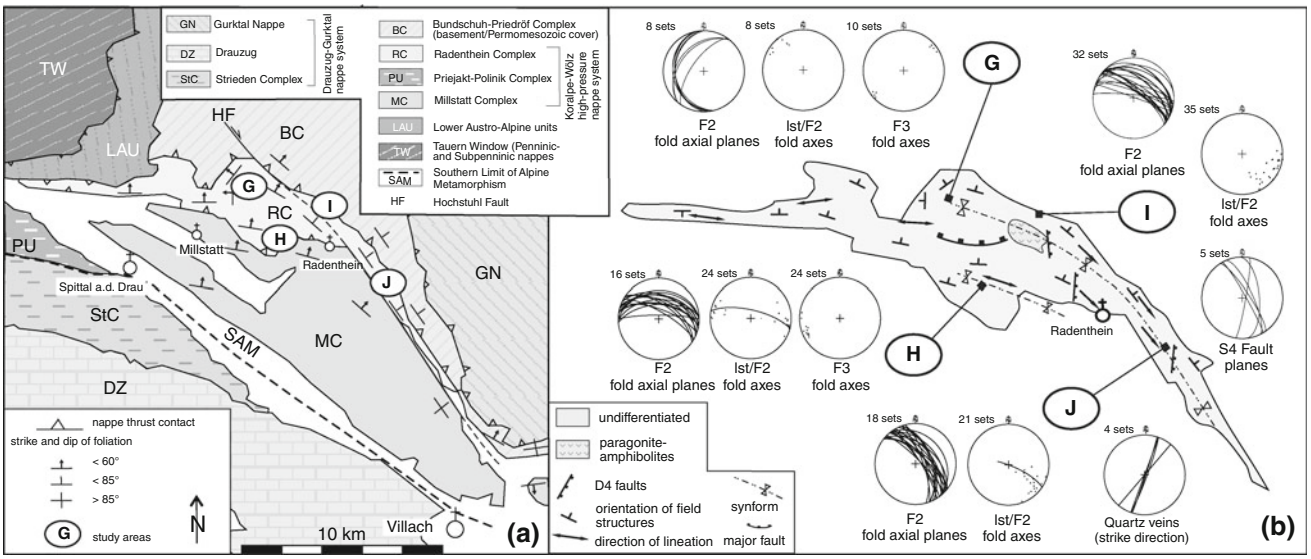

Fig. 4 **a** Tectonic map of the area southeast of the Tauern Window. Selected study areas G–J in the Radenthein Complex are indicated. **b** Structures within the study areas are plotted as lower hemisphere streographic projections

According to the structural evolution the RC shows strong similarities to the SC and is characterized by fold interferences with NW–SE and NE–SW trending fold axes. This would suggest one or more large-scale synforms characteristic for the internal structure of the RC. Like the SC, the overall shape of the RC displays large-scale bending of earlier structures.

4 Microstructures

4.1 West of the Tauern Window

Microstructures from micaschists at study area B (Seewer valley) suggest an early phase of quartz recrystallization. These fabrics were isoclinally folded, attributed to folding stage F1 (Fig. 6a). F1 folds and the associated foliation S1 occur enclosed in garnet cores and are surrounded by an external matrix foliation S2 consisting of fine-grained white mica (Fig. 6a, b). Two generations of biotite occur: biotite Bt1 always rotated parallel to S2 or aligned along early folds F1 and biotite (Bt2) which overgrew all earlier structures. Bt1 contains pumpellyite (Pmp) interpreted as a relic of an early prograde stage (Krenn et al. 2004). Microstructures related to garnet growth indicate three stages: stage I related to the syn-tectonic growth of garnet cores which led to a curved internal fabric S1 as well as to folds F1. S1 contains aligned coarse-grained ilmenite and tourmaline (Fig. 6c). Fabric asymmetry suggests WNW-directed shearing (deformation stage D1). This sense of shear is additionally supported by D2 strain-caps in the matrix (arrow in Fig. 6d). Symmetric pressure shadows are frequent and surround garnet porphyroblasts (Fig. 6d). S2 is often overgrown by inclusion-free garnet rims, defining growth stage II (Fig. 6c, d). Subsequent garnet resorption to Bt2 and later chlorite close to the rims defines growth stage III. Both minerals crystallized as thick patchy flakes and overgrew S2 and symmetric pressure shadows.

F2 folded granitoid gneisses show similar features. Beside growth zone I, post-tectonic growth of garnet rims (growth zone II) is also preserved (Fig. 6e). Garnets from these rocks show an oblique internal fabric S1 of recrystallized quartz grains which are smaller in size compared to the external fabric S2 of recrystallized quartz and feldspar. Feldspar is mostly affected by retrogression into fine grained sericitic mica.

In study area D/2, post-tectonic growth of garnet rims is missing (Fig. 6f). There, the internal fabric of the garnets suggests garnet growth during NW-directed shearing (D1) followed by the development of symmetric pressure shadows (D2). Due to the lack of garnet growth zone II, an angle of >90° between S1 and S2 is observed. S2 is overgrown by chlorite flakes (growth zone III).

4.2 East of the Tauern Window

Similar to the SC, isoclinal folds F1 and an associated foliation S1 are surrounded by a foliation S2 consisting of folded white mica (Fig. 7a). Patchy biotite flakes (Bt2) partly overgrew S2. Growth stages are comparable to the growth stages of the SC. On the basis of curved inclusion patterns in core domains of garnet poikiloblasts, growth stage I is associated with NW-directed shearing (deformation stage D1) (Fig. 7b). Inclusion-free garnet rims

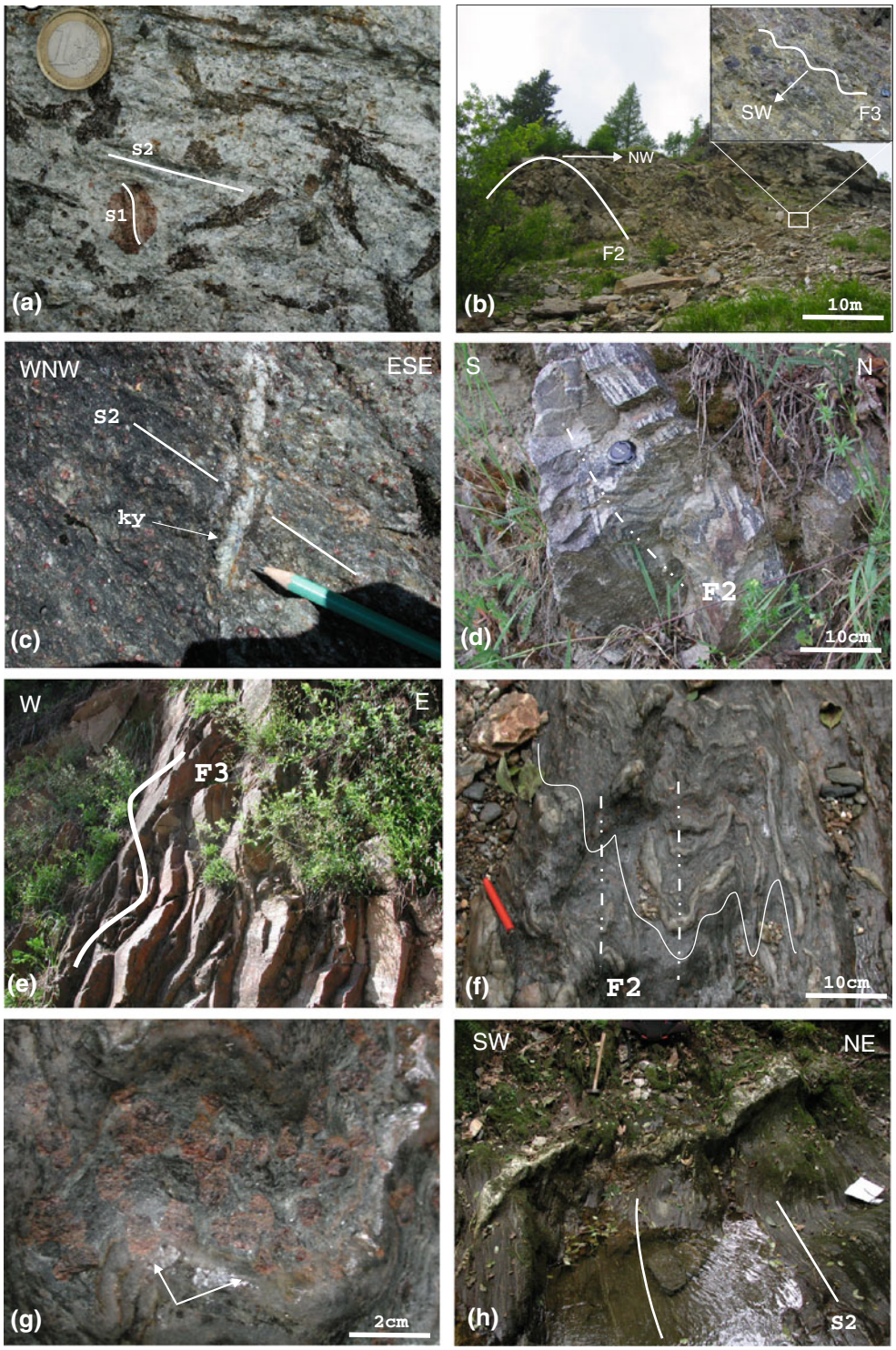

Fig. 5 **a** Quartzitic gneisses containing garnet poikiloblasts with D1 internal foliation and D2-postdeformative mineral growth of hornblende aggregates retrogressed to biotite. Photo taken from Hoinkes et al. (2010). **b** Large-scale (F2) and small-scale open (F3) folds at study area G. Note, different plunge directions between F2 and F3. **c** D2-postdeformative kyanite-bearing quartz veins (study area G). **d** Non-cylindrical intrafolial fold structure F2 within metabasic gneisses at study area H. **e** F3-open folds at study area H. **f** M-shape of intrafolial folds F2 within garnet-bearing gneisses at study area J. **g** D2-postdeformative mineral growth of garnet rims at the fold hinges of F2 folds (detail in **f**). **h** Large-scale quartz vein formed due to NW–SE-directed extension (study area I)

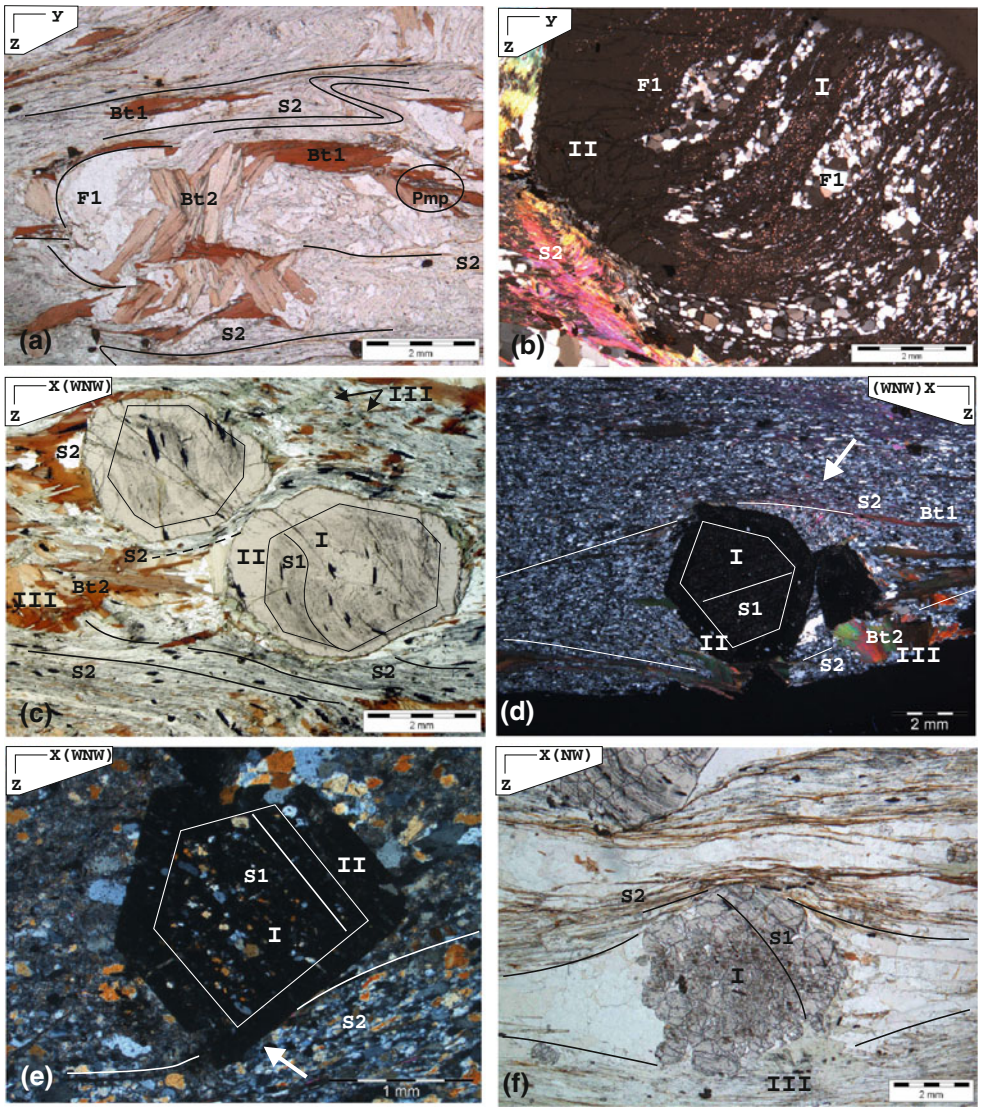

Fig. 6 Micro-scale structures of selected samples of the SC. **a** Isoclinal fold F1 and Bt1 including pumpellyite. Folded S2 planes were overgrown by Bt2 (micaschists, study area B/1). **b** Garnet poikiloblast contains F1 folds as inclusion patterns. F1 consist of recrystallized quartz with straight grain boundaries (garnet growth stage I). Inclusion-free garnet rims (growth stage II) are bordered by intensely folded white mica (S2). **c** Garnet porphyroblasts with S1-sigmoidal inclusion patterns of graphite and ilmenite suggest growth during WNW-directed shearing (D1). Cores are surrounded by inclusion-free rims (growth stage II). Symmetric pressures shadows around the porphyroblasts are overgrown by Bt2, postdeformative to S2 (micaschists, study area B/1). **d** Garnet-bearing quartzitic gneisses with comparable structural features like (**c**) (study area B/1). **e** Euhedral garnet poikiloblast shows D2-postdeformative rim growth. **f** Garnet porphyroblast with D1-sigmoidal inclusion pattern. Garnets are surrounded by symmetric pressures shadows (D2) and by postdeformative mineral growth of biotite retrogressed to chlorite (growth stage III). The lack of growth stage II results into a high angle between S1 and S2 (metapelites, study area D/2)

contain locally a straight fabric which continues into the external matrix foliation S2. It characterizes strain caps overgrown during garnet growth stage II. The external foliation S2 surrounds symmetric pressure shadows aligned by biotite (Bt1) and white mica. Postkinematic growth of Bt2 defines mineral growth stage III (Fig. 7a).

In study area H, retrogression in garnet-amphibolites is associated with the development of symmetric pressure shadows consisting of recrystallized quartz and plagioclase, aligned by hornblende aggregates (Fig. 7c). The internal fabric of these garnets suggests garnet growth during WNW-directed shearing.

In study area I, crystallization of garnet during WNW-directed shearing formed agglomerates with asymmetric shape (Fig. 7d). Additionally, asymmetric mica fish in quartzitic gneisses indicate W-directed shearing (Fig. 7e).

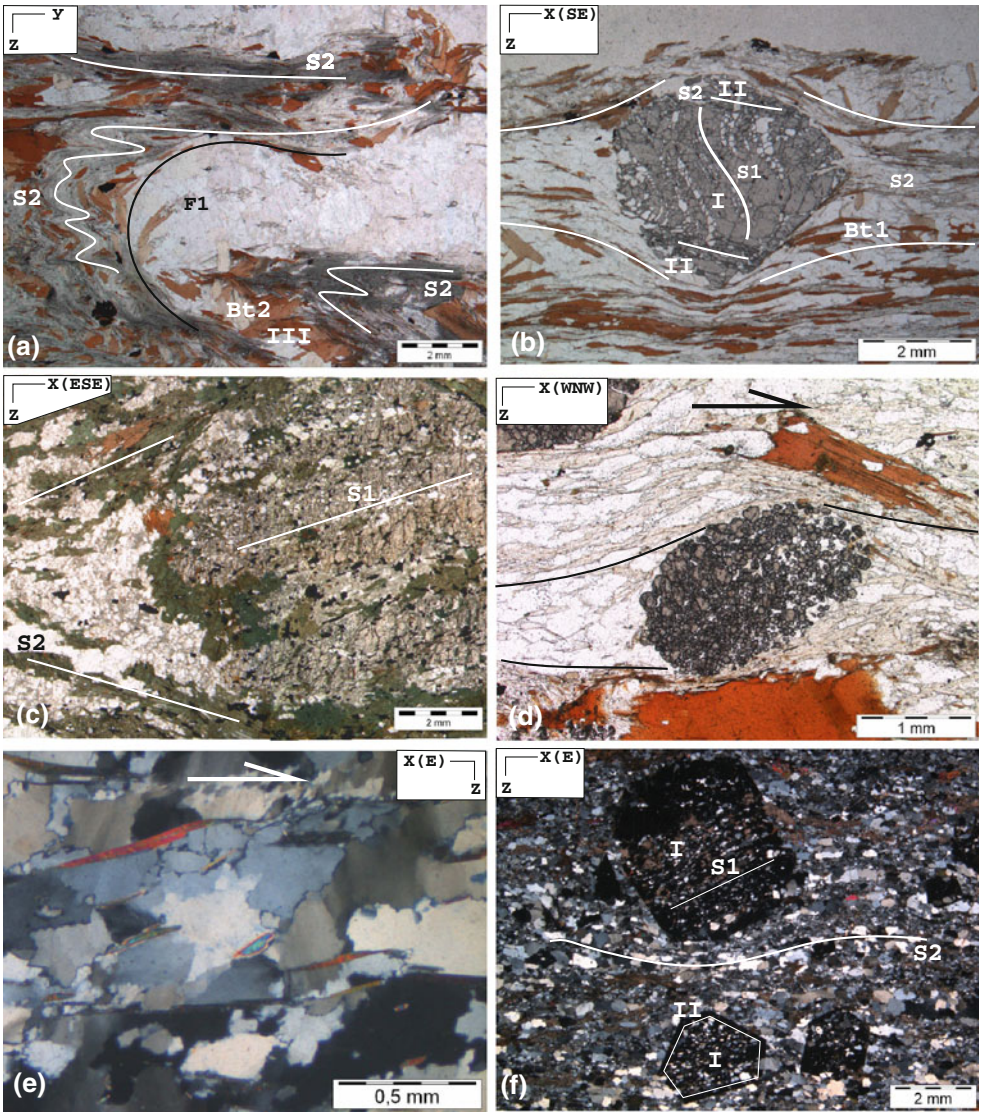

Fig. 7 Micro-scale structures of selected samples of the RC. **a** D1 structures (isoclinal fold F1) surrounded by the folded foliation S2 and by the late growth of Bt2 (growth stage III) (study area J). **b** Garnet poikiloblast with sigmoidal inclusion patterns (growth stage I) suggest growth during NW-directed shearing. Foliation S2 is enclosed in garnet rims (growth stage II) and continues into the external matrix foliation S2 (study area J). **c** Metabasite contains garnet with an internal foliation S1 surrounded by a pressure shadow aligned by hornblende crystals (study area H). **d** Garnet aggregates with asymmetric shape suggest crystallization during WNW-directed shearing (D1). **e** Mica fishes within the recrystallized quartz matrix indicate shearing to the W (study area I). **f** Garnet poikiloblasts show growth stages I and II. Inclusion patterns in growth stage I consist of recrystallized quartz and carbonate (study area J)

In study area J, garnets from quartzitic gneisses contain an earlier internal fabric S1 consisting of recrystallized quartz and carbonate grains (Fig. 7f). S1, oblique to the external foliation S2, indicates rotational garnet growth during W-directed shearing (growth stage I). Subsequent growth of small garnet rims (stage II) resulted in almost euhedral-shaped garnet aggregates. Compared to quartz grains in the cores of garnets, matrix quartz grains are larger in size and define together with mica and carbonate foliation S2.

5 Lattice preferred orientations

5.1 Analytical procedure

Lattice preferred orientations (LPOs) provide indirect information on syn-deformational temperature conditions, the kinematics of the associated flow (e.g. Lister and Hobbs 1980; Schmid and Casey 1986), the flow geometry and the flow vorticity (e.g. Vissers 1989; Law et al. 1990; Wallis 1992). X-ray texture goniometry (wavelength

CuKa = 1.5418, beam current = 40 kV and 40 mA) used in reflection mode was applied on polished rock chips at the Institute of Earth Sciences, University of Graz. Eight lattice planes ([100], [110], [102], [200], [201], [112], [211], [113]) of quartz were measured directly. Lattice planes [001], [101] and [011] were calculated using the orientation density function (ODF) on the basis of the harmonic method by Roe (1965) and Bunge (1981). For detailed description of the technical procedure see also Wenk (1985). From the asymmetry of <c> and <a> axes of quartz LPOs with respect to the foliation, the sense of shear was determined. From the symmetry of quartz <c> axes, i.e. oblique single girdle distribution versus cross girdle distribution, the dominance of non-coaxial or coaxial flow was qualitatively constrained.

Representative <c> axes [001] and <a> axes [110] distribution from the SC and RC are given as pole figures in Fig. 8a, b, respectively.

5.2 West of the Tauern Window

Five representative quartz samples were selected and are shown in Fig. 8a. Samples were taken from an F2 intrafolial fold limb in the "Bunte Randserie" of the SC (7SZ1, study area B/1), nearby the transition between the Ötztal nappe and the "Bunte Randserie" of the SC (7SZ7, study area B/2), from the Ötztal nappe in the south (PF22, study area D/1), from the fold hinge area of the Schrottner Synform in the SC (HW2, study area D/2) and near the southeastern marble unit of the TC (HW15, study area E).

All samples taken from the SC (7SZ1, 7SZ7, HW2) consist of recrystallized quartz aggregates that deformed due to dislocation creep and show intracrystalline grain boundary migration recrystallization (GBM). This suggests deformation temperatures of ≥550°C (e.g. Hirth and Tullis 1992, 1994). Quartz grains in samples taken from the Ötztal nappe (PF22) and near the marble unit (HW15) show bulging recrystallization processes (BLG), indicative for lower temperatures of <450°C (e.g. Hirth and Tullis 1994).

LPOs of 7SZ1 indicate a slight asymmetric small circle distribution of <c> axes [001] around z (Fig. 8a). <A> axes [110] show a small circle distribution close to the x–y plane. This pattern indicates flattening strain (Lister and Hobbs 1980). A probable asymmetry suggests shearing towards E against the plunge direction of the stretching lineation. By contrast, LPOs of sample 7SZ7 indicate NW-directed shearing at high temperature conditions given by the combination of prism <a> and rhomb <a> gliding. This is indicated by <c> axes [001] maxima in y and maxima between the center and the periphery of the pole figure. Microstructures of both samples show recrystallized quartz aggregates with almost equal grain size of ca. 200 µm (Fig. 9a, b). However, sample 7SZ7 (Fig. 9b) consists of grains with lobate grain boundaries contrasting to sample 7SZ1 (Fig. 9a) where straight grain boundaries, indicative for the dominance of static annealing, occur.

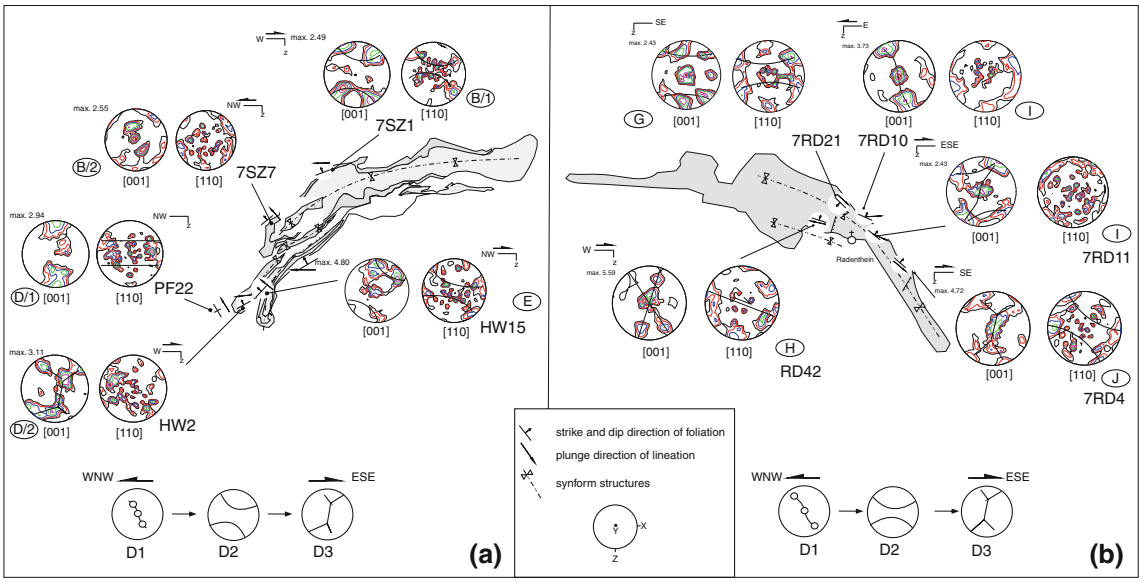

Fig. 8 Representative LPOs of the studied areas of the SC (**a**) and RC (**b**). In all pole figures the x–y plane defines the trace of the foliation in sections cut parallel to the stretching lineation and perpendicular to the foliation (see legend in the *box*). The field reference system of the pole figures is indicated. The *number on the upper left corner* of the pole figures corresponds to the maximum contours of multiples of random distribution

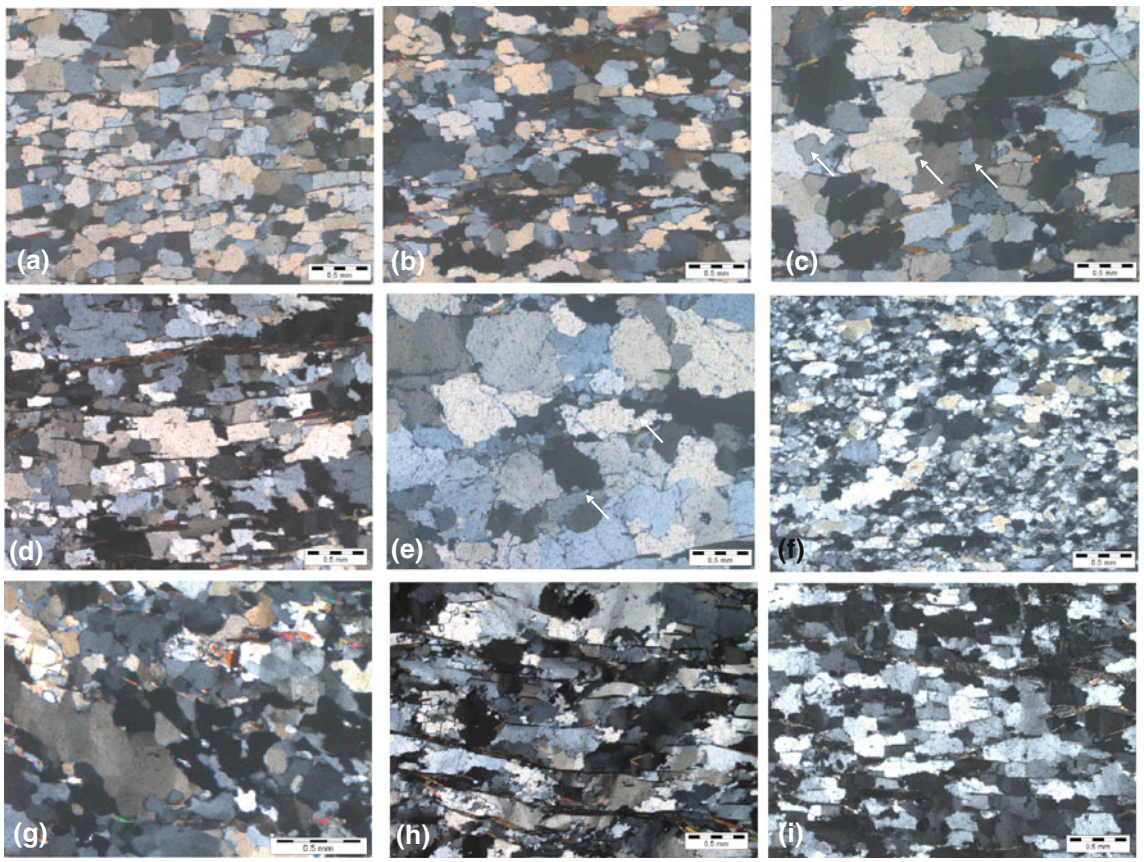

Fig. 9 Microstructures of selected quartzitic samples. **a** Recrystallized quartz grains with equal grain size and dominant straight grain boundaries (sample 7SZ1). **b** Recrystallized quartz grains equal grain size and dominant lobate grain boundaries (sample 7SZ7). **c** Quartz grains deformed by dominant bulging. Bulges and subgrains are indicated by *arrows* (sample PF22). **d** Recrystallized quartz grains with almost equal size and lobate grain boundaries (sample HW2). **e** Large quartz grains deformed by dominant bulging (*arrows* indicate bulges) (sample HW15). **f** Recrystallized quartz grains with lobate grain boundaries and almost equal size (sample 7RD21). **g** Large quartz grains with undulatory extinction surrounded by smaller recrystallized quartz grains indicating core-mantle textures (sample RD42). *Dark areas* indicate vertical quartz <c> axes. **h** Quartz grains unequal in size showing undulatory extinction and dominant bulging (sample 7RD10). **i** Recrystallized quartz grains with equal size and lobate grain boundaries (sample 7RD11)

LPOs of sample PF22 show dominant basal <a> gliding as evident from <c> axes [001] maxima around z and a girdle distribution of <a> axes [110] in the x–y plane (Fig. 8a). Quartz grains are larger in size (~500 µm) and show BLG being indicative for low-grade deformation conditions (Fig. 9c). LPOs and microstructures suggest dominant coaxial flow at conditions of about 350–400°C representative for the deformation geometry within the Ötztal nappe nearby the SC.

LPOs of sample HW2 show a slight asymmetric type I cross-girdle distribution as defined by Lister and Hobbs (1980), suggesting eastward shearing combined with coaxial flow (general shear) within the southernmost Schrottner Synform of the SC (Fig. 8a). Quartz grains are unequally sized between 200 and 500 µm and show mainly lobate grain boundaries indicative for GBM (Fig. 9d).

Sample HW15 was cut slightly oblique to the foliation and therefore appears irregular. LPOs are, however, similar to sample 7SZ1 with asymmetric small girdle distributions around z of <c> [001] and <a> axes [110] (Fig. 8a). Quartz grains are large in size (about 500 µm) and indicate dominance of BLG (Fig. 9e). Enhancement of grain size probably relies to the fact that secondary phases like mica, which limit recrystallization in sample 7SZ1, are absent. Asymmetry suggests shearing to SE, against the plunge direction of the stretching lineation.

5.3 East of the Tauern Window

Five representative LPOs for the RC are shown in Fig. 8b. Quartz samples were selected from the northern margin of the RC at study area G (sample 7RD21), from an F2-folded quartz layer at the southern part adjacent to the Millstatt Complex at study area H (sample RD42), nearby the transition zone between the RC and the Bundschuh nappe (samples 7RD10) and the inner part of the RC (sample

7RD11) at study area I and from an F2 intrafolial fold at the south-eastern RC (study area J; sample 7RD4).

LPOs from sample 7RD21 show a small circle distribution of <c> [001] and <a> [110] axes as indicative for flattening strain (Fig. 8b). No clear asymmetry is observed. Recrystallized quartz aggregates have lobate grain boundaries, are indicating GBM and minor BLG and show a size of about 200–500 μm (Fig. 9f).

LPOs of sample RD42 represent a type I crossed girdle distribution of <c> axes [001] (Fig. 8b). The asymmetry of the <a> axes [110] pattern suggests shearing to the E. Recrystallized quartz grains are up to 1 mm in size and indicate dominant BLG and subgrain rotation recrystallization (SGR) which suggests deformation during temperature conditions of ≤450°C (e.g. Hirth and Tullis 1994) (Fig. 9g).

LPOs of sample 7RD10 show an asymmetric girdle distribution by the combination of prism <a> and basal <a> ± rhomb <a> gliding. Asymmetry indicates W-directed shearing against the plunge direction of the stretching lineation, also supported by the presence of asymmetric mica fish (Fig. 7e). Quartz microstructures show dominant BLG and undulatory extinction with relics of GBM. Grain size is about 250–500 μm (Fig. 9h).

LPOs of sample 7RD11 show a combination of a small circle distributions of <c> axes [001] around z combined with low-grade basal <a> glide towards ESE. The small circle distribution results from flattening strain (Fig. 8b). Quartz microstructures show recrystallized quartz aggregates with almost equal size of ca. 250–500 μm (Fig. 9i). Dominant recrystallization mechanism is GBM with some amount of static annealing as indicated by straight grain boundaries.

LPOs of sample 7RD4 show an asymmetric type I cross-girdle distribution after Lister and Hobbs (1980) and suggest coaxial flow combined with SE-directed shearing (general shear) within the southernmost part of the RC (Fig. 8b). Quartz grains show a wide range of grain size (100–500 μm) and microstructures are indicative for a decreasing trend in deformational temperatures ranging from GBM over BLG to undulatory extinction (Fig. 7f).

5.4 Summary about LPOs and structures west and east of the Tauern Window

LPOs from quartz samples indicate coherent deformation geometries in the study areas west and east of the Tauern Window and can be linked with macro- to micro-scale deformation stages.

Deformation stage D1 is related to WNW-directed shearing under high temperature conditions (GBM: ≥550°C) and associated with an asymmetric girdle distribution diagnostic for prism <a> and basal <a> ± rhomb <a> slip. The shearing direction under high grade conditions correlates well with growth stage I of the studied garnet porphyroblasts. Representative samples were taken near the transition areas from the SC to the Ötztal nappe and from the RC to the Bundschuh nappe, respectively.

Deformation stage D2 and D3 evolved under high- to medium-temperature conditions (GBM and minor BLG: ca. 450–550°C) with local annealing textures. It is characterized by coaxial flow defined by small girdle distributions of <c> [001] and <a> axes [110] with minor asymmetries towards the E. This trend is additionally supported by asymmetric type-I cross-girdles with asymmetries probably pointing to a combination of coaxial flow and E-directed simple shearing at comparable temperature conditions. Coaxial flow can be linked with the observed F2 and F3 folding stages and the development of symmetric pressure shadows around garnet porphyroblasts surrounded by foliation S2. Additional asymmetries are correlated with minor shearing related to E-directed extension. Subsequent growth of garnet rims (growth stage II) and minerals may be linked to the observed annealing textures.

Locally preserved D4 structures are only studied at macro-scale and not analysed by LPO textures.

6 Tectonic model for the evolution of the SC and RC

The SC and RC derived either from Paleozoic or from Permian to Triassic carbonatic to clastic sedimentary sequences, as proposed by Puhr et al. (2009) or as previously suggested by Justin-Visentin and Zanettin (1965) and Zanettin and Justin-Visentin (1971). These sedimentary sequences were deposited on older basement units, which were intruded by magmatites of Permian age and which now constitute the Texel and Millstatt Complexes (Schuster and Stüwe 2008; see Fig. 10a). All of these four complexes are parts of the Eoalpine high-pressure wedge (after Schmid et al. 2004) and were exhumed between ca. 90 Ma (peak metamorphic conditions; e.g. Thöni et al. 2008) and ca. 70–60 Ma (cooling of the Texel Complex below 300°C at ~70 Ma: Habler et al. 2006; cooling of the Ötztal nappe below 100°C at ~60 Ma: Fügenschuh et al. 2000).

It is proposed that thrusting of parts of the highest tectonic units, i.e. the Steinach and Gurktal nappe as members of the DGN, occurred during an earlier stage of Alpine nappe stacking, i.e. during phase 1 at >115 Ma, before the onset of subduction of the future Eoalpine high-pressure wedge (Fig. 10a). Arguments about the relative tectonic position of the Ötztal–Bundschuh nappe system (ÖBN), which might be either structurally below or above the Koralpe–Wölz high-pressure wedge, are as follows. The southern parts of the ÖBN share a common

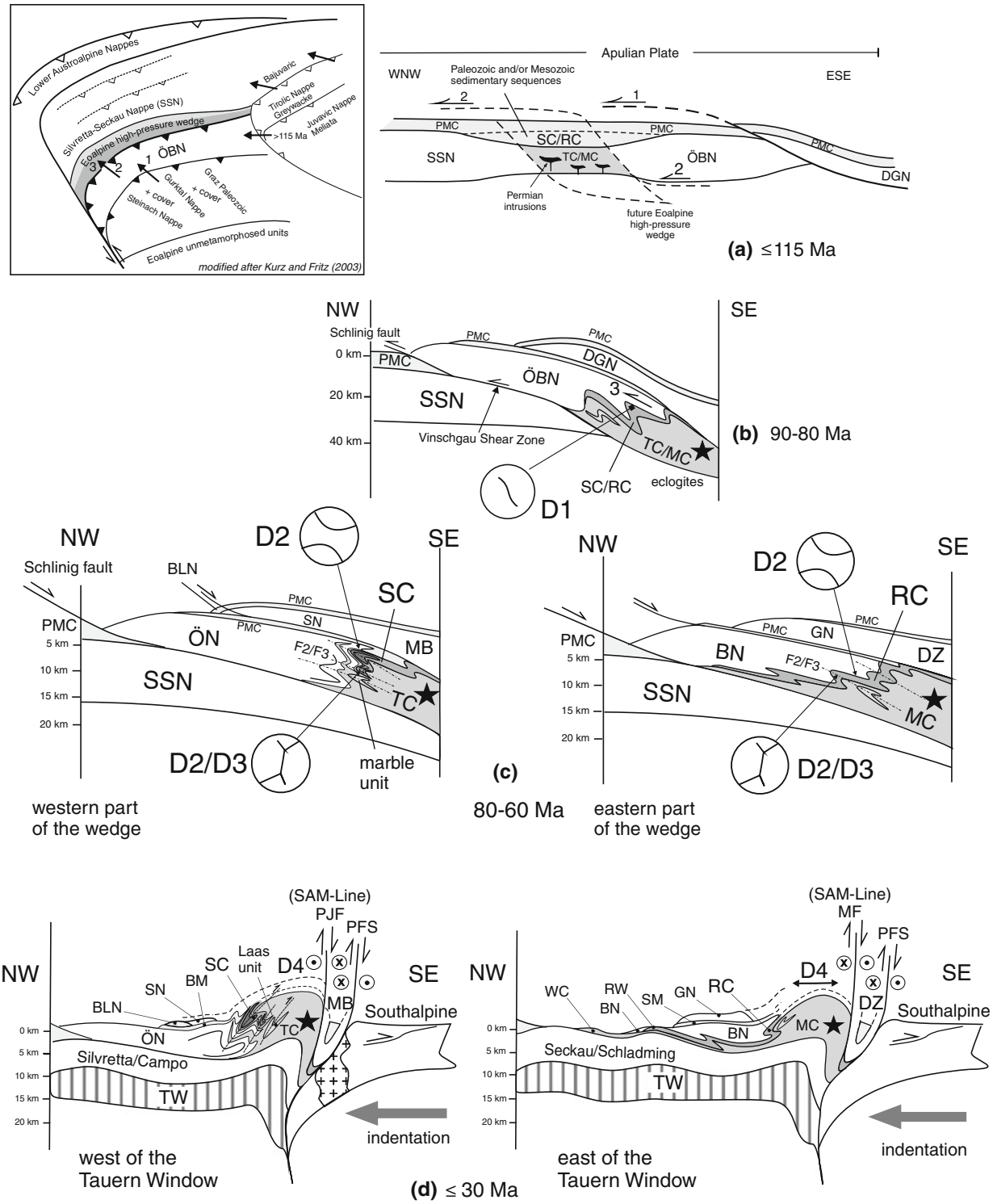

Fig. 10 Model for the tectonic evolution of Austroalpine nappes from Early Cretaceous to Late Paleogene times. Representative LPOs are linked with distinct deformation stages. Sketches are not to scale. *Upper box* includes a paleogeographic sketch (*left*) with the relative positions of Austroalpine nappes during Late Jurassic–Mid Cretaceous times (modified after Kurz and Fritz 2003). *SSN* Silvretta Seckau nappe system, *ÖBN* Ötztal–Bundschuh nappe system, *TC/MC* Texel/Millstatt Complex, *SC/RC* Schneeberg/Radenthein Complex, *PMC* Permo-Mesozoic cover sequences, *DGN* Drauzug–Gurktal nappe system, *ÖN* Ötztal nappe, *SN* Steinach nappe, *BM* Brenner Mesozoic, *SC* Schneeberg Complex, *TC* Texel Complex, *PJF* Passeier–Jaufen Fault, *MB* Meran-Mauls Basement, *PFS* Periadriatic Fault System, *BN* Bundschuh nappe, *SM* Stangalm Mesozoic, *RC* Radenthein Complex, *MC* Millstatt Complex, *RW* Rammingstein Window, *WC* Wölz Complex, *GN* Gurktal nappe, *DZ* Drauzug, *StC* Strieden Complex, *SAM-Line* Southern Limit of Alpine Metamorphism, *MF* Mölltal Fault

tectonometamorphic evolution with the high-pressure wedge. This favours a lower plate position where the parts of the ÖBN were incorporated into Eoalpine continental subduction. However, the Bundschuh nappe, now located east of the Tauern Window, is seen to be underlain by the high-pressure wedge of the RC (Fig. 4a) and by high-pressure units in the Rammingstein area ("Rammingstein Window" RW in Fig. 1) that contain "monometamorphic" garnet mica schists (Schuster and Frank 1999). This clearly implies a tectonic position of the ÖBN above the high-pressure wedge, and the latter therefore is representing a relatively higher nappe system (Fig. 10b). The ÖBN has been folded together with the SC/RC and TC/MC during exhumation (Fig. 10c). Deformation was accompanied by Eoalpine mineral growth at the base of the ÖBN (new growth of Eoalpine staurolite in the SC and retrogression of pre-Eoalpine staurolite into fine-grained white mica in the ÖBN) (e.g. Hoinkes 1981; Hoinkes et al. 1999; Schuster and Frank 1999).

WNW-directed shearing is observed both west and east of the Tauern Window and is compatible with the overall kinematics during Eoalpine nappe stacking (e.g. Ratschbacher 1986; Ratschbacher and Neubauer 1989; Linzer et al. 1995; Neubauer et al. 2000; Kurz and Fritz 2003). In the SC, prograde to peak metamorphic conditions are linked with the static growth of poikiloblastic garnets, followed by syn-kinematic growth during WNW-directed shearing (D1) under early retrograde conditions (Krenn 2010). This study shows that this also applies to the RC. Peak metamorphic conditions for the SC and RC were calculated between 550 and 600°C at ca. 10 kbar (Konzett and Hoinkes 1996; Koroknai et al. 1999; Krenn 2010). Sm-Nd data indicate garnet growth in the SC (Bunte Randserie) at 93.1 ± 4.7 Ma (Sölva et al. 2005). Garnet growth during eclogite facies metamorphism in the Texel Complex is about 85 ± 5 Ma (Habler et al. 2006). Both age data constrain the lower time limit for SE-directed continental subduction (Fig. 10b).

Thrusting of the upper plate (ÖBN and DGN) towards NW is defined as stacking phase 2 and occurred slightly earlier than phase 3 which is characterized by the rapid exhumation of the high-pressure wedge. Hence the base of the upper plate was incorporated into early and subsequent folding stages which resulted into the formation of large-scale F2/F3 fold interferences, incorporating the south-eastern ÖBN and the TC/MC in the front of the exhuming wedge (Fig. 10c). F2/F3 fold patterns formed the synform structures and produced the so-called "Schlingentektonik". It is proposed that this pattern evolved in the part of the wedge west of the Tauern window, but it is not verified in detail in the east. East of the Tauern window RC and MC have been thrusted further towards NW onto the lower plate (Silvretta–Seckau nappe system).

Orientations of F2 intrafolial folds in the SC are comparable to the orientations of fold axes in the Texel Complex studied by Sölva et al. (2001) and folding stages F2 and F3 are therefore related to this advanced exhumation stage. On the micro-scale, symmetric strain shadows around garnets developed at a minimum crustal depth of ca. 12 km (~4 kbar) and ca. 550–600°C (Krenn 2010).

During exhumation of the wedge, evidence for the early stage of WNW-directed shearing is additionally supported by non-coaxial fabrics (D1) that pass progressively into pure shear. Coaxial deformation (D2 and D3) is associated with the advanced stage of exhumation and affected both, the ÖBN and the high-pressure wedge beneath (Fig. 10c).

It is proposed that exhumation was accompanied by NW–SE-directed extension along a system of normal faults which reactivated earlier thrusts in the front of the wedge. The Schlinig Fault is interpreted as a former W-directed thrust system (Schmid and Haas 1989 reactivated during E-directed normal faulting (Froitzheim et al. 1997). Stacking phase 3 is therefore accommodated by thrusting along the Schlinig Fault and the Vinschgau Shear Zone at the base of the ÖBN (Fig. 10b).

Another former thrust system reactivated by normal faulting during Late Cretaceous times was that between the ÖBN and its cover (Brenner and Stangalm Mesozoic) (e.g., Koroknai et al. 1999; Fügenschuh et al. 2000). This led to final cooling of the ÖBN and to advanced exhumation of the high-pressure wedge beneath. In both our study areas SE-directed extension correlates with coaxial LPO textures which indicate subvertical flattening within the SC and the RC (Fig. 10c).

The late stages of exhumation coincided with heat advection towards shallow crustal levels, raising the overall geotherm. This is evident from post-kinematic growth of garnet rims and hornblende garben. Field observations suggest that this late-stage mineral growth is dominant in the fold hinge areas of the main synforms, probably indicating fluid controlled mineral growth along S2 fold axial planes. Crustal extension and normal faulting probably caused condensed isotherms, e.g. at the transition between the ÖBN and the SC/RC. Post-kinematic mineral growth is observed in study areas B/1, B/2 and D/2 of the SC and in study areas G, H and J of the RC.

The current orientations of the dip direction of the main foliation (towards the N and NW in the SC, and towards the N and NE in the RC) are considered to have resulted from tilting induced by the indentation of the Southalpine units as the frontal parts of the NE-dipping Adriatic plate during Oligocene to Miocene times (Kissling et al. 2006; Brückl et al. 2010; see Fig. 10d). Indentation led to significant rotation of the main foliation and all lithotectonic boundaries at the front of the wedge from the original south- to the present-day northward dip linked with semiductile to

brittle overprinting, mainly observed in the southern parts of the SC and RC (D4). Adjacent to the Periadriatic Fault, the uppermost units of the Eoalpine nappe pile (DGN) were verticalized and locally overturned and finally juxtaposed with the high-pressure units as a result of N-side-up displacement along the Passeier–Jaufen Fault and the Mölltal Fault (PJF and MF in Fig. 10d). This late-stage folding and faulting formed a southernmost large-scale synform containing Triassic cover in its core: the Meran-Mauls basement with Triassic marbles in the west (MB in Fig. 10d) and the Strieden Complex (StC) and Drauzug in the east (DZ in Fig. 10d). The SAM-Line simply follows the Passeier–Jaufen and Mölltal Faults.

During D4, oblique convergence released a set of semiductile to brittle faults with north-side up displacement accompanied with a change from sinistral to dextral displacement during Oligocene/Early Miocene times along the PJF (e.g., Spiess 1995; Müller et al. 2001; Mancktelow et al. 2001; Viola et al. 2003). Displacements are compatible with N–S to NNW–SSE shortening and orogen-parallel extension and linked with S4 planes in the southern part of the SC that are parallel to the strike of the PJF. In the RC, WNW–ESE extension is linked with the formation of large discordant quartz veins and D4 fault planes. Due to unroofing of Penninic and Subpenninic units within the Tauern Window the SC and RC were laterally separated into a western and eastern unit, respectively (e.g., Frisch et al. 2000).

The high-pressure units further in the east (Koralpe–Saualpe) with dominantly S-dipping foliation planes contrast with the N-dipping foliations found within the SC and RC (Fig. 1). Hence, before the D4 low-grade overprint, Early Cretaceous thrust-related structures formed by N- to NW-directed shearing and folding (D1–D3) in the internal parts of the high-pressure wedge. This is compatible with Eoalpine structures found in the eastern parts of the Eastern Alps (Kurz and Fritz 2003). Coaxial geometries with no clear shear sense are proposed for the Plattengneis shear zone of the Koralpe which is interpreted as a flat-lying synmetamorphic shear zone (e.g. Krohe 1987; Kurz et al. 2002). It is therefore suggested that the units of the high-pressure nappe system, after an earlier stage of non-coaxial shearing, experienced dominant coaxial flow with flattening strain geometries during exhumation. The Koralpe–Saualpe, however, was not affected by south-alpine indentation like the SC and RC and therefore remained in their approximate orientation since consolidation of the Eoalpine nappe stack.

7 Conclusions

This study supports previous interpretations (e.g., Frisch et al. 2000) about a common tectonothermal evolution of Alpine monometamorphic units west and east of the Tauern Window. Comparisons of structures and metamorphic grades within the high-pressure nappe system south of the pre-Alpine basement of the Ötztal–Bundschuh nappe system indicate that both units were closely related before tectonic unroofing of Penninic and Subpenninic units within the Tauern Window. The observed micro- and macro-scale structures from both study areas developed during exhumation of the high-pressure wedge, controlled by NW directed shearing (D1) and extrusion (D2–D3) between $\geq$90 and 60 Ma. The low-grade D4 overprint under semiductile/brittle conditions observed in the SC and RC is interpreted as resulting from overall shortening and lateral slip due to the indentation of the Adriatic plate in Oligocene–Miocene times. Transpression (shearing and folding) led to intense bending and steepening of the foliation planes during SW directed brittle shearing, mainly in the SC, and brittle overprinting, mainly in the RC. The current strike direction of the main foliation in the southernmost SC and RC, which is almost NE–SW and NW–SE, respectively, results from block rotation accompanied with strike-slip faulting during Miocene times. Strike-slip was sinistral with north-side-up displacement in the southern part of the SC along the PJF, and dextral in the RC along the Mölltal Fault (MF) at its southern margin and along the Hochstuhl Fault (HF) at its northern margin (e.g. Polinski and Eisbacher 1992; Mancktelow et al. 2001) (Fig. 1).

Based on considering the effects of indentation it is argued that the SC west of the Tauern Window, previously interpreted to represent a wide shear zone accommodating normal displacements (Schneeberg Normal Fault Zone) (Sölva et al. 2005), is an area formed by rotated and originally S-dipping and NW-directed thrust-related fabrics. NW-directed normal shearing is only apparent and resulted from lower crustal indentation. The SC is part of a sedimentary sequence of Paleozoic or Mesozoic depositional age that was squeezed between intensely folded polymetamorphic basement rocks.

The coherence of the thrust-related structures throughout the Koralpe–Wölz high pressure nappe system of the Eastern Alps implies that structures related to nappe stacking and extension during Cretaceous time were originally identical in the areas west and east of the Tauern Window. The current tectonostratigraphy of basement/cover nappes resulted from three different stacking events, which evolved during time increments (stacking events 1–3 in Fig. 10). Transpression accompanied by tectonic erosion formed the high-pressure wedge below the ÖBN, which is overlain by the Steinach and Gurktal nappes including their respective Permo-Mesozoic cover sequences.

Acknowledgments This study mostly benefits from the intense field work during the past years which was partly financially supported by

the Austrian Science Fund FWF P-14728 to G. Hoinkes. The authors would like to thank two reviewers (W. Frisch and R. Schuster) and co-editor S. Schmid for their fruitful critics and suggestions. Comments from R. Schuster and S. Schmid improved the manuscript significantly.

References

Belocky, R. (1987). Strukturgeologische Untersuchungen in Kristallin und Gurktaler Decke im Raum Radenthein-Bad Kleinkirchheim (Nockgebiet/Kärnten/Österreich). Unpubl. Diploma Thesis, University Vienna, Vienna.

Bernhard, F., Klötzli, U. S., Thöni, M., & Hoinkes, G. (1996). Age, origin and geodynamic significance of a polymetamorphic felsic intrusion in the Ötztal Crystalline Basement, Tirol, Austria. *Mineralogy and Petrology*, *58*, 171–196.

Brückl, E. et al. (2010). Crustal structure and active tectonics in the Eastern Alps. *Tectonics*, 29, TC2011. doi:10.1029/2009TC002491.

Bunge, H. J. (1981). Fabric analyses by orientation distribution functions. *Tectonophysics, 78*, 1–21.

Faryad, S. W., & Hoinkes, G. (2003). P-T gradient of Eo-Alpine metamorphism within the Austroalpine basement units east of the Tauern Window (Austria). *Mineralogy and Petrology, 77*, 129–159.

Frank, W., Hoinkes, G., Purtscheller, F., & Thöni, M. (1987). The Austroalpine Unit West of the Hohe Tauern: The Ötztal–Stubai Complex as an example for the Eoalpine metamorphic evolution. In: W. Flügel & P. Faupl (Eds.), *Geodynamics of the Eastern Alps* (pp. 179–225). Vienna: Deuticke.

Frimmel, H. (1987). Isotopengeologische Hinweise auf die paläogeographische Nachbarschaft von Gurktaler Decke (Oberostalpin) und dem Altkristallin östlich der Hohen Tauern (Österreich). *Schweizerische Mineralogische und Petrographische Mitteilungen, 66*, 193–208.

Frimmel, H. (1988). Metagranitoide am Westrand der Gurktaler Decke (Oberostalpin)—Genese und paläotektonische Implikation. *Jahrbuch der Geologischen Bundesanstalt, 131*, 575–592.

Frisch, W., Dunkl, I., & Kuhlemann, J. (2000). Post-collisional orogen-parallel large-scale extension in the Eastern Alps. *Tectonophysics, 327*, 239–265.

Froitzheim, N., Conti, P., & van Daalen, M. (1997). Late Cretaceous, synorogenic, low-angle normal faulting along the Schlining fault (Switzerland, Italy, Austria) and its significance for the tectonics of the Eastern Alps. *Tectonophysics, 280*, 267–293.

Froitzheim, N., Schmid, S. M., & Conti, P. (1994). Repeated change from crustal shortening to orogen—parallel extension in the Austroalpine units of Graubünden. *Eclogae geologicae Helvetiae, 87*, 559–612.

Fügenschuh, B., Mancktelow, N. S., & Seward, D. (2000). Cretaceous to Neogene cooling and exhumation history of the Oetztal–Stubai basement complex, Eastern Alps; a structural and fission track study. *Tectonics, 19*, 905–918.

Genser, J., & Neubauer, F. (1989). Low angle normal faults at the eastern margin of the Tauern Window (Eastern Alps). *Mitteilungen der Österreichischen Geologischen Gesellschaft, 81*, 233–243.

Habler, G., Thöni, M., & Sölva, H. (2006). Tracing the high pressure stage in the polymetamorphic Texel Complex (Austroalpine basement unit, Eastern Alps): P–T–t–d constraints. *Mineralogy and Petrology, 88*, 269–296.

Hawkesworth, C. J. (1976). Rb/Sr geochronology in the Eastern Alps. *Contributions to Mineralogy and Petrology, 54*, 225–244.

Helbig, P., & Schmidt, K. (1978). Zur Tektonik und Petrogenese am W-Ende des Schneeberger Zuges (Ostalpen). *Jahrbuch der Geologischen Bundesanstalt, 121*, 177–217.

Hirth, G., & Tullis, J. (1992). Dislocation creep regimes in quartz aggregates. *Journal of Structural Geology, 14*, 145–159.

Hirth, G., & Tullis, J. (1994). The brittle-plastic transition in experimentally deformed quartz aggregates. *Journal of Geophysical Research, 99*, 11731–11747.

Hoinkes, G. (1981). Mineralreaktionen und Metamorphosebedingungen in Metapeliten des westlichen Schneebergerzuges und des angrenzenden Altkristallins (Ötztaler Alpen). *Tschermacks Mineralogisch Petrographische Mitteilungen, 28*, 31–54.

Hoinkes, G. (1986). Effect of grossular-content in garnet on the partitioning of Fe and Mg between garnet and biotite. An empirical investigation on staurolite-zone samples from the Austroalpine Schneeberg complex. *Contributions to Mineralogy and Petrology, 92*, 393–399.

Hoinkes, G., Höller, F., Rantitsch, G., Dachs, E., Höck, V., Neubauer, F., et al. (1999). Alpine metamorphism of the Eastern Alps. *Schweizer Mineralogische und Petrographische Mitteilungen, 79*, 155–181.

Hoinkes, G., Koller, F., Demény, A., Schuster, R., Miller, Ch., Thöni, M., et al. (2010). Metamorphism in the Eastern Alps. *Acta Mineralogica-Petrographica, Field Guide Series, 1*, 1–47.

Hoinkes, G., Kostner, A., & Thöni, M. (1991). Petrologic constraints for eo-Alpine eclogite facies metamorphism in the Austroalpine Ötztal Basement. *Mineralogy and Petrology, 43*, 237–254.

Janák, M., Froitzheim, N., Lupták, B., Vrabec, M., & Krogh Ravna, E. J. (2004). First evidence for ultrahigh-pressure metamorphism of Eclogites in Pohorje, Slovenia: Tracing deep continental subduction in the eastern Alps. *Tectonics*, 23, TC5014. doi:10.1029/2004TC001641.

Justin-Visentin, E., & Zanettin, B. (1965). Gli scisti cristallini dell'alta Val Passiria fra Moso e Passo del Rombo (Alto Adige). *R. C. Soc. Mineral. Ital*., 21.

Kaindl, R., & Abart, R. (2002). Reequilibration of fluid inclusions in garnet and kyanite from metapelites of the Radenthein Complex, Austroalpine Basement, Austria. *Schweizerische Mineralogische und Petrographische Mitteilungen, 82*, 467–486.

Kaindl, R., Hoinkes, G., Knoll, P., & Abart, R. (1999). Fluid inclusions related to Variscan and Alpine metamorphism in the Austroalpine Ötztal Basement, Eastern Alps. *Mineralogy and Petrology, 65*, 29–49.

Kissling, E., Schmid, S. M., Lippitsch, R. Ansorge, J., & Fügenschuh, B. (2006). Lithosphere structure and tectonic evolution of the Alpine arc: new evidence from high-resolution teleseismic tomography. In: D. G. Gee & R. A. Stephenson (Eds.), *European lithosphere dynamics* (Vol. 32, pp. 129–145). Memoirs: Geological Society of London.

Klötzli-Chowanetz, E., Klötzli, U. S., & Koller, F. (1997). Lower Ordovician migmatisation in the Ötztal crystalline basement (Austria): Linking U/Pb and Pb–Pb dating with zircon morphology. *Schweizerische Mineralogische und Petrographische Mitteilungen, 77*, 315–324.

Konzett, J., & Hoinkes, G. (1996). Paragonite-hornblende assemblages and their petrological significance: An example from the Austroalpine Schneeberg Complex, Southern Tyrol, Italy. *Journal of Metamorphic Geology, 14*, 85–101.

Koroknai, B., Neubauer, F., Genser, J., & Topa, D. (1999). Metamorphic and tectonic evolution of Austroalpine units at the western margin of the Gurktal nappe complex, Eastern Alps. *Schweizerische Mineralogische und Petrographische Mitteilungen, 79*, 277–295.

Krenn, K. (2010). Fluid inclusions in quartz related to subsequent stages of foliation development during a single metamorphic

cycle (Schneeberg Fault Zone, Eastern Alps, Austria). *Lithos, 118*, 255–268.

Krenn, K., Kaindl, R., & Hoinkes, G. (2004). Pumpellyite in metapelites of the Schneeberg Complex (Eastern Alps, Austria): A relict of the eo-Alpine prograde P-T-path? *European Journal of Mineralogy, 16*, 661–669.

Krohe, A. (1987). Kinematics of Cretaceous nappe tectonics in the Austroalpine basement of the Koralpe region (eastern Austria). *Tectonophysics, 136*, 171–196.

Kurz, W., & Fritz, H. (2003). Tectonometamorphic evolution of the Austroalpine Nappe Complex in the central Eastern Alps–consequences for the Eo-Alpine evolution of the Eastern Alps. *International Geology Review, 45*, 1100–11127.

Kurz, W., Fritz, H., Tenczer, V., & Unzog, W. (2002). Tectonometamorphic evolution of the Koralm Complex (Eastern Alps): Constraints from microstructures and textures of the "Plattengneis"—shear zone. *Journal of Structural Geology, 24*, 1957–1970.

Law, R. D., Schmid, S. M., & Wheeler, J. (1990). Simple shear deformation and quartz crystallographic fabrics: A possible natural example from the Torridon area of NW Scotland. *Journal of Structural Geology, 12*, 29–54.

Linzer, H. G., Ratschbacher, L., & Frisch, W. (1995). Transpressional collision structures in the upper crust: The fold-thrust belt of the Northern calcareous Alps. *Tectonophysics, 242*, 41–61.

Lippitsch, R., Kissling, E., & Ansorge, J. (2003). Upper mantle structure beneath the Alpine orogen from high-resolution teleseismic tomography. *Journal of Geophysical Research*, 108, 2002JB002016.

Lister, G. S., & Hobbs, B. E. (1980). The simulation of fabric developments during plastic deformation and its application to quartzite: The influence of deformation history. *Journal of Structural Geology, 2*, 355–370.

Liu, Y., Genser, J., Handler, R., Friedl, G., & Neubauer, F. (2001). $^{40}Ar/^{39}Ar$ muscovite ages from the Penninic-Austroalpine plate boundary, Eastern Alps. *Tectonics*, *20*, 526–547.

Mancktelow, N. S., Stöckli, D. F., Grollimund, B., Müller, W., Fügenschuh, B., Viola, G., Seward, D., & Villa, I. M. (2001). The DAV and Periadriatic fault systems in the Eastern Alps south of the Tauern window. *International Journal of Earth Science*, 90, 593–622.

Mauracher, J. (1980). *Alpidische und voralpidische Metamorphose und Strukturprägung am Westende des Schneeberger Zuges (Ötztaler Alpen)*. Unpublished PhD Thesis, Vienna University, Vienna.

Miller, Ch., & Thöni, M. (1995). Origin of eclogites from the Austroalpine Ötztal basement (Tirol, Austria): Geochemistry and Sm-Nd vs. Rb-Sr isotope systematics. *Chemical Geology*, 122, 199–225.

Müller, W., Prosser, G., Mancktelow, N. S., Villa, I., Kelley, S. P., Viola, G., et al. (2001). Geochronological constraints on the evolution of the Periadriatic Fault System (Alps). *International Journal of Earth Science (Geologische Rundschau)*, *90*, 623–653.

Neubauer, F., Frisch, W. B. T., & Hansen, B. T. (1987). Time relations between Eoalpine metamorphism and thrusting: Evidence from the crystalline basement of the eastern Greywacke Zone. In: H. W. Flügel & P. Faupl (Eds.), *Geodynamics of the Eastern Alps* (pp. 263–271). Vienna: Deuticke.

Neubauer, F., Genser, J., & Handler, R. (2000). The Eastern Alps: Result of a two-stage collision process. *Mitteilungen der Österreichischen Geologischen Gesellschaft*, *92*, 117–134.

Neubauer, F., Hoinkes, G., Sassi, F. P., Handler, R., Höck, V., Koller, F., et al. (1999). Pre-Alpine metamorphism of the Eastern Alps. *Schweizerische Mineralogische Petrographische Mitteilungen, 79*, 41–62.

Oberhauser, R. (1980). *Der Geologische Aufbau Österreichs*. Wien: Geologische Bundesanstalt.

Polinski, R. F., & Eisbacher, G. H. (1992). Deformation partitioning during polyphase oblique convergence in the Karawanken Mountains, southeastern Alps. *Journal of Structural Geology*, *14*, 1203–1213.

Puhr, B., Hoinkes, G., Proyer, A., & Schuster, R. (2009). Petrology of metacarbonate rocks of the Austroalpine basement east of the Tauern Window (Austria). *Mitteilungen der Österreichischen Mineralogischen Gesellschaft*, 155, p. 134.

Purtscheller, F. (1978). Ötztaler und Stubaier Alpen. *Sammlung Geologischer Führer* 53, 2. Aufl., Gebrüder Borntraeger, Berlin.

Purtscheller, F., & Rammlmair, D. (1982). Alpine Metamorphism of Diabase dikes in the Ötztal–Stubai Metamorphic Complex. *Tschermacks Mineralogische Petrographische Mitteilungen*, *29*, 205–221.

Ramsay, J. G., & Huber, M. I. (1987). *The techniques of modern structural geology* (Vol. 2). London: Academic Press.

Ratschbacher, L. (1986). Kinematics of Austroalpine cover nappes: Changing translation to transpression. *Tectonophysics*, *125*, 335–356.

Ratschbacher, L., & Neubauer, F. (1989). West-directed decollement of Austro-Alpine cover nappes in the eastern Alps: Geometrical and rheological considerations. In: M. P. Coward, D. Dietrich & R. G. Park (Eds.), *Alpine tectonics* (pp. 243–262). Geological Society Special Publication, London.

Roe, R. J. (1965). Description of crystallite orientation in polycrystalline materials. III. General solution to the pole figure inversion. *Journal of Applied Physics*, *36*, 2024–2031.

Schimana, R. (1986). *Geologische Entwicklung des Kristallins in der Umgebung um Radenthein (Nockgebirge/Kärnten)*. Unpublished PhD Thesis. University Vienna, Vienna.

Schmid, S. M., & Casey, M. (1986). Complete fabric analysis of some commonly observed quartz c-axis patterns. *Geophysical Monography*, *36*, 263–286.

Schmid, S. M., Fügenschuh, B., Kissling, E., & Schuster, R. (2004). Tectonic map and overall architecture of the Alpine orogen. *Eclogae geologicae Helvetiae*, *97*, 93–117.

Schmid, S. M., & Haas, R. (1989). Transition from near surface thrusting to intrabasement decollement, Schlinig thrust, Eastern Alps. *Tectonics*, *8*, 697–718.

Schmidegg, O. (1964). *Die Ötztale Schubmasse und ihre Umgebung* (pp. 27–47). Wien: Verhandlungen der geologischen Bundesanstalt.

Schuster, R., & Frank, W. (1999). Metamorphic evolution of the Austroalpine units east of the Tauern Window: Implications for Jurassic strike-slip tectonics. *Mitteilungen der Gesellschaft der Geologie-und Bergbaustudenten Österreichs*, *42*, 37–58.

Schuster, R., Koller, F., Hoeck, V., Hoinkes, G., & Bousquet, R. (2004). Explanatory notes to the map: Metamorphic structure of the Alps–Metamorphic evolution of the Eastern Alps. *Mitteilungen der Österreichischen Mineralogischen Gesellschaft, 149*, 175–199.

Schuster, R., & Stüwe, K. (2008). Permian metamorphic event in the Alps. *Geology*, *36*, 603–606.

Sölva, H., Grasemann, B., Thöni, M., Thiede, R., & Habler, G. (2005). The Schneeberg Normal Fault Zone: Normal faulting associated with Cretaceous SE-directed extrusion in the Eastern Alps (Italy, Austria). *Tectonophysics, 401*, 143–166.

Sölva, H., Thöni, M., Grasemann, B., & Linner, M. (2001). Emplacement of eo-Alpine high-pressure rocks in the Austroalpine Ötztal complex (Texel group, Italy/Austria). *Geodinamica Acta*, *14*, 345–360.

Spiess, R. (1995). The Passeier–Jaufen Line: A tectonic boundary between Variscan and an eo-Alpine Meran-Mauls basement. *Schweizerische Mineralogische Petrographische Mitteilungen*, *75*, 413–425.

Teiml, X., & Hoinkes, G. (1996). Der P-T Pfad d3er Millstätter Serie und ein Vergleich mit dem südlichen Ötztal–Stubai–Kristallin. *Mitteilungen der Österreichischen Mineralogischen Gesellschaft*, *141*, 228–229.

Teiml, X., Hoinkes, G., & Konzett, J. (1995). Joint occurrence of eclogites and white mica-amphibolites in the Austroalpine Basement (Eastern Alps). *Terra Nova*, Abstracts Suppl., 1, 318.

Thöni, M. (1981). Degree and evolution of the Alpine Metamorphism in the Austroalpine Unit W of the Tauern Window in light of K/Ar and Rb/Sr age determinations on Micas. *Jahrbuch der Geologischen Bundesanstalt*, *124*, 111–174.

Thöni, M. (1999). A review of geochronological data from the Eastern Alps. *Schweizerische Mineralogisch Petrographische Mitteilungen*, *79*, 209–230.

Thöni, M., Miller, C., Blichert-Toft, J., Whitehouse, M. J., Konzett, J., & Zanetti, A. (2008). Timing of high-pressure metamorphism and exhumation of the eclogite type-locality (Kupplerbrunn–Prickler Halt, Saualpe, south-eastern Austria): Constraints from correlations of the Sm-Nd, Lu-Hf, U-Pb and Rb-Sr isotopic systems. *Journal of Metamorphic Geology*, *26*, 561–581.

Tollmann, A. (1977). *Geologie von Österreich. Band 1*. Wien: Die Zentralalpen.

Tropper, P., & Hoinkes, G. (1996). Geothermobarometry of Al2SiO5 bearing metapelites in the western Austroalpine Ötztal basement. *Mineralogy and Petrology*, *58*, 145–170.

Viola, G., Mancktelow, N., Seward, D., Meier, A., & Martin, S. (2003). The Pejo fault system; an example of multiple tectonic activity in the Italian Eastern Alps. *Geological Society of America Bulletin*, *115*, 515–532.

Vissers, R. L. M. (1989). Asymmetric quartz c-axis fabric and flow vorticity: A study using rotated garnets. *Journal of Structural Geology*, *11*, 231–244.

Wallis, S. R. (1992). Vorticity analysis in a metachert from the Sanbagawa Belt, SW Japan. *Journal of Structural Geology, 14*, 271–280.

Wenk, H. R. (1985). Measurements of pole figures. In: H. R. Wenk (Eds.), *An introduction to modern texture analysis* (pp. 11–47). Orlando: Academic Press.

Wiesinger, M., Neubauer, F., & Handler, R. (2006). Exhumation of the Saualpe eclogite unit, Eastern Alps: Constraints from $^{40}Ar/^{39}Ar$ ages and structural investigations. *Mineralogy and Petrology, 88*, 149–180.

Zanchetta, S., Salvi, F., Zanchi, A., & Poli, S. (2007). Structural aspects of the Texel–Schneeberg boundary in the Pfossen valley (Central-Eastern Alps, NE Italy). *Mitteilungen der Österreichischen Mineralogischen Gesellschaft* 153.

Zanchi, A., Francesca, S., Stefano, Z., Simone, S., & Graziano, G. (2009). 3D reconstruction of complex geological bodies: Examples from the Alps. *Computers and Geosciences, 35*, 49–69.

Zanettin, B., & Justin-Visentin, E. (1971). *Considerzioni Geologico-Petrologiche Sul "tratto di Monteneve" ("Schneeberger Gesteinszug") (Alto Adige)*. Padova: Mem. Ist. Geol. e Miner. Univ. Padova.